IV. 研究成果の刊行物・別冊

総　説

人工血小板開発の現状と今後の展望

慶應義塾大学医学部輸血・細胞療法センター

半田　　誠　Makoto HANDA

はじめに

我が国では急速な少子高齢化に伴い，献血人口の減少と悪性腫瘍などの増加による輸血需要が高まり，近い将来の血液製剤の払底が危惧されており，それを代替する人工血液の開発が進められてきた。厳密な取扱いを要する輸血用血液製剤のなかでもとりわけ血小板濃厚液は，その機能を保持するために，室温（22℃），水平震盪条件下で保存しなければならず，その有効期限も採血後4～7日（我が国は4日）と短い。従って，血小板濃厚液を医療現場で常備することは事実上不可能（我が国では予約制）であり，災害や事故，産科的領域に合併した突発的な大量出血に緊急対応することは極めて困難である。血小板製剤の欠点を克服し，長期保存可能で常時使用できる人工物の開発が，米国において主に軍事目的で始まってからすでに50年以上が経過した[1,2]。残念ながら，未だ実用化には至っていないが，幾つかの有望な試験物が報告され，一部は初期臨床試験に供され，将来の製剤化への取組みが継続されている[2,3]。血小板の止血機能や血小板輸血の適応と対比して，人工血小板の開発の現状と今後の展望を概説する。

人工血小板の設計戦略

1．血小板の作用機序（図1）

血小板の最も重要な生理機能は，止血カスケードにおいて1次血栓を形成し，さらに凝固系の活性化を仲介してフィブリンによる強固な2次血栓を誘導することである。実際，血管壁の破綻により露出したコラーゲンなどの内皮下組織成分やそこに特異的に集積した血漿のフォン・ビレブランド因子（以下，VWF）をリガンドとして，血小板はその表面にある接着因子受容体（それぞれ，GPVIとGPIb/IX複合体）を介して認識して，止血部位に集積し，その表面を覆うように伸展する（血小板粘着）。活性化された血小板は，アデノシン2リン酸（以下，ADP）などの顆粒内容物を放出し，トロンボキサンA2を産生して，さらに強力な活性化を受けるとともに，活性化依存性の受容体であるGPIIb/IIIa複合体（$\alpha IIb\beta 3$インテグリン）とそのリガンドの血漿フィブリノゲンが結合して，互いに架橋を形成することで血小板凝集が惹起され，1次血栓が形成される（血小板放出反応と血小板凝集）。活性化された血小板の表面にはフォスファチジルセリンなどの陰性荷電を有するリン脂質が露出して，その表面で凝固カスケードが爆発的に進行し，トロンビンの産生に伴うフィブリン血栓の形成が誘導され（血小板凝固活性），止血血栓が完成する。

2．人工血小板の設計戦略

生きた血小板を模して，上記の複雑に連動した一連の細胞反応を人工的に創出することは事実上不可能である。幸いに，血小板輸血が必要な場合でも患者の血小板が全くゼロになることはない。そこで，人工血小板として，止血局所に集積する残存血小板に働いて，著しく低下している1次止血機能を増強する薬物をつくり出すことが現実的かつ合理的である。すなわち，人工血小板は血小板の代わりとなるものではなく，あくまでも血小板の機
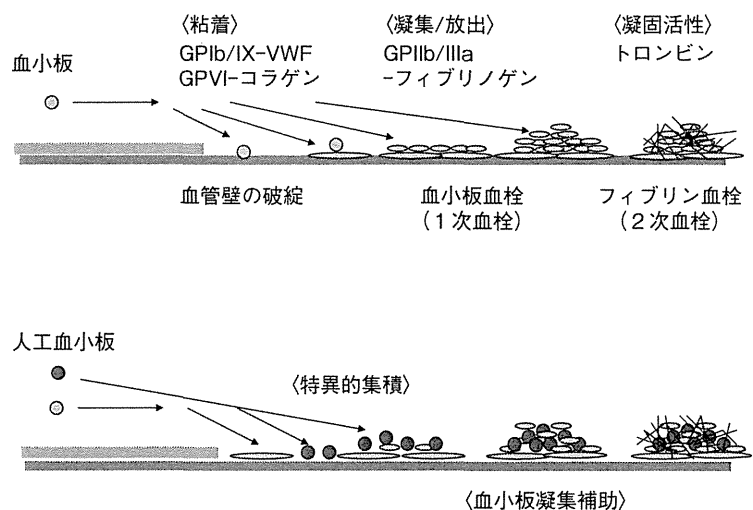

図1　止血血栓の形成と人工血小板の機能

能を補強もしくは増強することで，血小板減少症や機能低下症などで障害されている1次止血機能を補助する（血小板代替薬）かあるいは止血機能を増強する薬剤（止血薬）として開発されている。

人工血小板創製への最初の試みは，フィブリノゲンあるいはその関連合成ペプチド（GPIIb/IIIa複合体結合部位）を共有結合で表面修飾したヒト赤血球である。フィブリノゲン結合赤血球は*in vitro*でアゴニスト惹起血小板凝集を用量依存性に増強し，血小板が減少したラットの延長した出血時間を短縮した[4]。フィブリノゲンのα鎖の2ヵ所に存在してGPIIb/IIIa複合体と特異的に結合する最少単位であるArginine-Glycine-Asparatic acid（以下，RGD）配列を含む合成ペプチド（CGCRGDF）が結合した赤血球（thromboerythrocyte）も同様の血小板凝集増強作用を認めた[5]。これらの修飾赤血球は，アゴニストにより活性化された血小板と，フィブリノゲンの活性化依存性受容体のGPIIb/IIIa複合体を介して選択的に結合することで，血小板血栓（血小板凝集）を増強する。これらの報告をきっかけとして，人工血小板として，流血中の活性化されていない血小板とは結合せずに，止血部位に集積した活性化血小板を特異的に認識する粒子を設計する方向性が確立された（図1）。すなわち，生体適合性に優れた担体を選択し，血中滞留時間をできるだけ延長させるためにポリエチレングリコール鎖（以下，PEG）で表面修飾し，活性化血小板を標的として，止血局所への特異的な集積を誘導するリガンドを結合させた微粒子の開発が次々と行われ，現在に至っている（図2）。リガンドとしてはフィブリノゲンあるいはその結合単位配列（RGDあるいはH12）を含んだ合成ペプチドが用いられている。
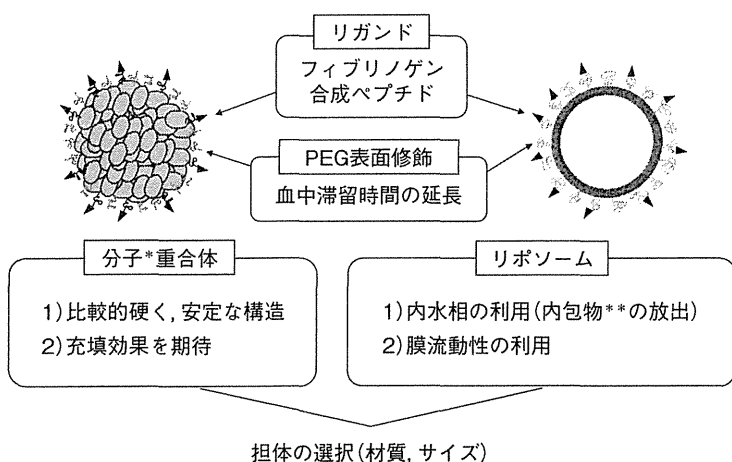
* ：ヒトアルブミン，PLGA
** ：ADP

図2　人工血小板の設計

人工血小板の開発状況
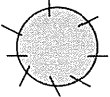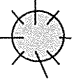
広義の人工血小板は，ヒト由来の血小板もしくはその断片を用いた血小板由来産物（platelet products）と，一部もしくはすべての構成成分が人工物であるいわゆる狭義の人工血小板（artificial platelets）に大別される[1~3]。前者には，凍結乾燥処理したヒト血小板（Stasix™，Thrombosomes™）と血小板膜断片（infusible platelet membrane：IPM）（Cyplex™）がある。後者は，担体としてアルブミン微粒子，リン脂質小胞体：リポソームおよびポリ乳酸/グリコール酸共重合体（poly (lactic-co-glycolic acid)：以下，PLGA）を用い，その表面にフィブリノゲンやその合成ペプチド（RGDあるいはH12）などをコートした微粒子が開発され，ヒトフィブリノゲンを表面固定したアルブミン微粒子（Synthocyte™やFibrinoplate-S™）が初期臨床試験に供された[2,3]。ヒト由来のアルブミン（遺伝子組換えアルブミンが開発されている）やフィブリノゲンを使用したものは生物由来製剤として規制を受けるため，開発の方向性は生物由来成分を一切使用しない完全型人工血小板にシフトしてきた（図3）。

1．フィブリノゲン結合アルブミン微粒子

1995年には，平均径が1.2μmのアルブミン・マイクロスフェア（Fibrinoplate-S™）が，1999年には，より大型の平均径3.5~4.5μmのアルブミン・マイクロカプセル（Synthocyte™）が報告され，前者はフェーズIII，後者は少なくともフェーズIIまでの臨床試験が行われた。特に，Fibrinoplate-S™は，63,214人の白血病や再生不良性貧血等の血小板減少患者（血小板数3万/μL以下）への二重盲検比較対照試験で，出血時間の短縮効果が投与後24時間後でも有意に持続することが報告された[6]。一方，Synthocyte™は，抗がん剤により惹起された血小板減少ウサギに投与することで耳介出血時間の短縮や腹部手術モデルでも術創からの出血量の減少効果が一定時間（3時間）持続し，止血局所への集積も形態的に証明され，有望な前臨床試験結果が公表された[7]。しかしながら，いずれもその後の経過の詳細は公表されておらず，未だ実用化に至っていない。さらに，第3の有望な人工物（HaemoPlax™）が開発されている。このHaemoPlax™は，アルブミン・マイクロスフェアの表面に，ヒトフィブリノゲンと高い親和性を有する合成ペプチドが固相

950

リガンド	担体/サイズ	製品名/報告者	適応	開発フェーズ
■血小板由来産物（凍結乾燥品）				
Lyophilized whole platelets		(Stasix™ : Entegrion) (Thrombosomes™ : Cellphire)	止血剤	前臨床
Platelet membrane fragments		Infusible Platelet Membrane (Cyplex™ : Cypress Bioscience)	予防, 治療	臨床 I / II （開発中止）
■人工血小板：リガンド結合微粒子				
Human Fibrinogen	Alb microcapsules (3.5-4.5μm)	(Synthocytes™ : ProFibrix)	予防, 治療	臨床 I / II （開発中止）
Human Fibrinogen	Alb microspheres (1.2μm)	(fibrinoplate-S™ : Advanced Therapeutics)	予防, 治療	臨床 II / III
		(HaemoPlax™ : Haemostatix)		前臨床
Human fibrinogen peptide (H12)	liposomes (0.22μm)	(Y. Okamura et al, 2005-2009) (Y. Nishikawa et al, 2012)	治療	前臨床
Human fibrinogen peptide (RGD)/VBP & CBP	liposomes (0.15μm)	(A. Sen Gupta et al, 2012)	止血剤	前臨床
Human fibrinogen peptide (RGD)	PLGA (0.17μm)	(J.P. Bertram et al, 2009)	止血剤	前臨床

（最下段3行を括る縦書き：完全型人工物）

VBP : VWF-binding peptide,　CBP : collagen-binding peptide

図3　人工血小板の開発状況

化されたもので，血中に投与すると，その表面にフィブリノゲンが速やかに吸着されることで，上記の人工物と同様の血小板代替機能を発揮するという。前臨床試験はすでに終了して，早期の臨床試験への移行を表明しているが，詳細は明らかでない。

2．フィブリノゲンペプチド結合ADP内包化リポソーム

　フィブリノゲンのGPIIb/IIIa複合体への結合部位は2ヵ所ある。1つはα鎖のRGD配列で，もう1つがγ鎖のカルボキシ末端を構成する12個のアミノ酸配列（[400]HHLGGAKQAGDV[411] : H12）である。そこで，表面結合リガンドとしてRGD配列の代わりにH12合成ペプチドを，担体として血液適合性に優れかつすでに臨床応用がなされているリポソームを使用した完全型人工血小板（H12（ADP）リポソーム）が開発された。RGD配列はGPIIb/IIIa複合体以外のインテグリン・ファミリーにも認識され，血小板への特異性は高くない。一方，H12はGPIIb/IIIa複合体に限定された結合部位であり，結合親和性は低いものの，活性化血小板への特異性は極めて高い。H12（ADP）リポソームは平均直径220nmのナノ微粒子で，その止血作用を強化する目的で細胞活性化とともに血小板より放出される生理的な血小板刺激物質のADPを内包化させている（図4）[8]。H12（ADP）リポソームは活性化した血小板に結合することで，出血部位に特異的に集積し，血小板凝集を増強するとともに，凝集依存性に内包化されたADPを放出することで，血小板に匹敵する止血効果（出血時間短縮効果）を発揮することが抗がん剤惹起ウサギ血小板減少症モデルで報告された。交通事故などの多発性外傷や臓器損傷に伴う大量出血は，血小板減少を伴って出血性ショックに陥りやすく，血小板輸血が必要となる。しかしながら，実際の医療現場では血小板製剤は入手困難であり，人工血小板のよい適応である。肝臓損傷による大量出血ウサギモデルでの検討では，H12（ADP）リポソームは血小板輸血と同等の止血効果と救命率を示した（図5）[9]。H12（ADP）リポソー
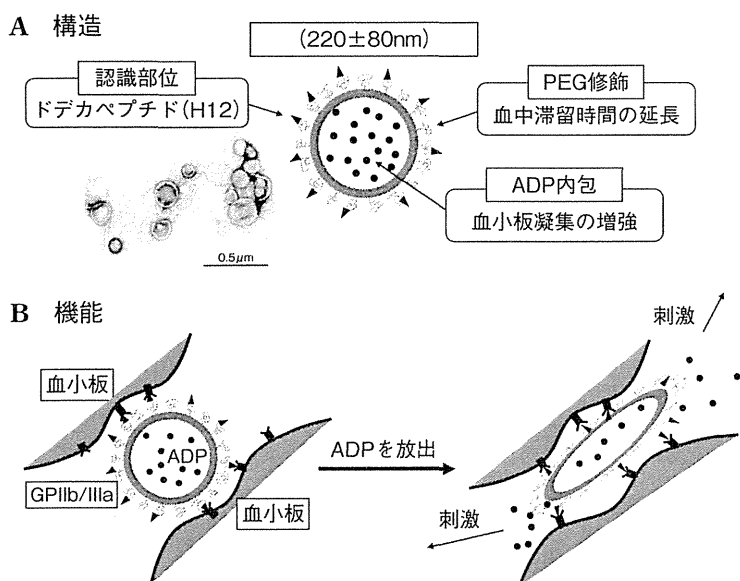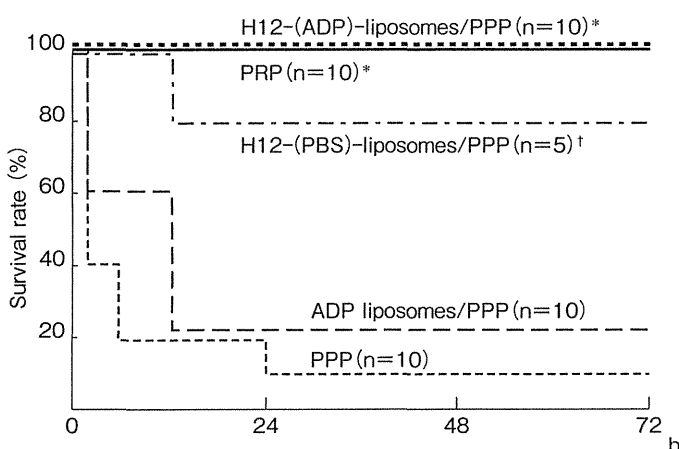
951

A　構造

| 認識部位 |
| ドデカペプチド（H12） |

（220±80nm）

| PEG修飾 |
| 血中滞留時間の延長 |

| ADP内包 |
| 血小板凝集の増強 |

0.5μm

B　機能

刺激

| 血小板 |

ADP

ADPを放出

| GPIIb/IIIa |

| 血小板 |

刺激

図4　H12（ADP）リポソーム

H12-(ADP)-liposomes/PPP(n=10)*

PRP(n=10)*

H12-(PBS)-liposomes/PPP(n=5)†

ADP liposomes/PPP(n=10)

PPP(n=10)

全血脱血と洗浄赤血球の返血を8回繰返し作成した稀釈性血小板減少症ウサギにH12（ADP）リポソーム（20mg/kg）と乏血小板血漿（PPP）を投与し，15分後に肝臓に貫通性損傷を与え，輸液のみの処置にて，動物の予後を観察。比較対照として，多血小板血漿（PRP），PPPのみ，H12未結合リポソーム（ADP-リポソーム）およびADP未内包リポソーム（H12-PBSリポソーム）を用いた。

*：p＜0.01 vs. PPP or ADPリポソーム，
†：p＜0.01 vs. PPP and p＜0.05 vs. ADPリポソーム

〈文献9）より引用〉

図5　肝臓外傷による大量出血ウサギモデルにおけるH12（ADP）
　　　リポソームの救命効果

ムの利点は，その表面をポリエチレングリコールで修飾することでその血中滞留時間を長く（平均6時間）でき，かつ肝臓などの臓器への蓄積性を認めないことである[10]。
3．多種類ペプチド結合リポソーム
　ナノ粒子であるPEG表面修飾リポソームに3種類の合成ペプチドを付加した多機能型の人工血小板が最近開発された[3,11]。活性化血小板への特異性を高めた環状RGDペプチドとともに，血小板粘着の標的分子であるコラゲ

ンとVWFの結合配列由来の合成ペプチド（それぞれCBPおよびVBP）を結合したリポソームは，血小板凝集増強機能ばかりでなく血小板粘着のプロセスにも直接関与して，血小板による止血機能を増強するとされる（図1）。実際，健常マウスの尾切出血時間を強力に短縮する作用が認められていることから，止血薬としての開発の方向性が示唆される。一方，血小板輸血の適応となる血小板減少症への効果については定かではない。
　4．フィブリノゲンペプチド結合低分子ポリマー
　この人工物は，生体吸収性に優れて多方面の医療材料に利用されているPLGAを担体として用い，その表面をPEGで修飾し，その先端にRGD配列を含んだペプチド（GRGDS）を結合させた，粒径およそ170nmの微粒子である[12]。本微粒子は，活性化した血小板にのみ結合して血小板の凝集を増強し，健常マウスの大腿動脈からの出血を陰性対照物に比して有意により短時間で止める機能がある。しかし，投与量を多くすると血栓傾向が増強されるとされ，また血中半減期も極めて短いことから，止血薬としての適応を目的としているようである。少なくとも，緊急避難的に止血薬として欧米では標準的に使用されているリコンビナント活性化凝固第VII因子（Novoseven[TM]）をはるかに凌駕する止血効果を示している。

今後の展望

　開発中の人工血小板の方向は，血小板代替薬か止血薬かである。血小板製剤に代わって何時でもどこでも使える長所がある反面，血小板を介してその機能が発揮されることから血小板が極端に減った状態で果たして機能するか未だに明らかでない点が不安材料である。さらに，止血予防を目的とした場合は時間的に余裕のあるためその効果が確実な血小板製剤でこと足りる。従って，外傷出血等で緊急に使用する場合に適応は限られ，利潤を追求する企業にとっては開発意欲が削がれる。一方，血小板数にかかわらず使用できる止血薬であれば，企業的なインセンティブも働く。ただし，安全性において止血機能亢進作用は血栓傾向増強作用と表裏一体である。従って，現時点では戦場での緊急避難的な適応が第1のターゲットとなっている。米国等の国防予算により支援

952

されたバイオベンチャーが開発を主導している現状から，詳細なデータはほとんど公表されていない。開発プロセスが公表されているのは，唯一我が国の公的資金の支援により開発が進められているH12（ADP）リポソームのみである。

引用文献

1) M.A. Blajchman : Substitutes and alternatives to platelet transfusions in thrombocytopenic patients, *J Thromb Haemost*, 1, 1637-1641 (2003).

2) 半田　誠：人工血小板, 脈管学, **51**, 333-378 (2011).

3) C.L. Modery-Pawlowski, L.L. Tian *et al.* : Approaches to synthetic platelet analogs, *Biomaterials*, **34**, 526-541 (2013).

4) G. Agam, A.A. Livine : Erythrocytes with covalently bound fibrinogen as a cellular replacement for the treatment of thrombocytopenia, *Eur J Clin Invest*, **22**, 105-112 (1992).

5) B.S. Coller, K.T. Springer *et al.* : Thromboerythrocytes, In vitro studies of a potential autologous, semi-artificial alternative to platelet transfusion, *J Clin Invest*, **89**, 546-555 (1992).

6) Advanced Therapeutics Inc. HP : http://www.advtx.com/Fibrinoplate-s-details.htm

7) M. Levi, P.W. Friedrich *et al.* : Fibrinogen-coated albumin microcapsules reduce bleeding in severely thrombocytopenic rabbits, *Nat Med*, **5**, 107-111 (1999).

8) 岡村陽介, 半田　誠：ナノ粒子と血小板の相互作用：完全人工系血小板代替物への応用を目指して, *International Review of Thrombosis*, **8**, 34-41 (2013).

9) K. Nishikawa, K. Hagisawa *et al.* : Fibrinogen γ-chain peptide-coated, ADP-encapsulated liposomes rescue thrombocytopenic rabbits from non-compressible liver hemorrhage, *J Thromb Haemost*, **10**, 2137-2148 (2012).

10) K. Taguchi, H. Ujihira *et al.* : Pharmacokinetic Study of the Structural Components of Adenosine Diphosphate-encapsulated Liposomes Coated with Fibrinogen γ-Chain Dodecapeptide as a Synthetic Platelet Substitute, *Drug Metab Dispos*, 2013 (in press).

11) C.L. Modery-Pawlowski, L.L. Tian *et al.* : In vitro and in vivo hemostatic capabilities of a functionally integrated platelet-mimetic liposomal nanoconstruct, *Biomaterials*, **34**, 3031-3041 (2013).

12) J.P. Bertram, C.A. Williams *et al.* : Intravenous hemostat: nanotechnology to halt bleeding, *Sci Transl Med*, **1**, 11-22 (2011).

953

Epitope Mapping for Monoclonal Antibody Reveals the Activation Mechanism for αVβ3 Integrin

Tetsuji Kamata[1]*, Makoto Handa[2], Sonomi Takakuwa[1], Yukiko Sato[1], Yohko Kawai[3], Yasuo Ikeda[4], Sadakazu Aiso[1]

1 Department of Anatomy, Keio University School of Medicine, Shinjuku-ku, Tokyo, Japan, 2 Center for Transfusion Medicine and Cell Therapy, Keio University School of Medicine, Shinjuku-ku, Tokyo, Japan, 3 Preventive Health Examination Center, International University of Health and Welfare, Minato-ku, Tokyo, Japan, 4 The Faculty of Science and Engineering, Graduate School of Advanced Science and Engineering, Waseda University, Shinjuku-ku, Tokyo, Japan

Abstract

Epitopes for a panel of anti-αVβ3 monoclonal antibodies (mAbs) were investigated to explore the activation mechanism of αVβ3 integrin. Experiments utilizing αV/αIIb domain-swapping chimeras revealed that among the nine mAbs tested, five recognized the ligand-binding β-propeller domain and four recognized the thigh domain, which is the upper leg of the αV chain. Interestingly, the four mAbs included function-blocking as well as non-functional mAbs, although they bound at a distance from the ligand-binding site. The epitopes for these four mAbs were further determined using human-to-mouse αV chimeras. Among the four, P3G8 recognized an amino acid residue, Ser-528, located on the side of the thigh domain, while AMF-7, M9, and P2W7 all recognized a common epitope, Ser-462, that was located close to the α-genu, where integrin makes a sharp bend in the crystal structure. Fibrinogen binding studies for cells expressing wild-type αVβ3 confirmed that AMF-7, M9, and P2W7 were inhibitory, while P3G8 was non-functional. However, these mAbs were all unable to block binding when αVβ3 was constrained in its extended conformation. These results suggest that AMF-7, M9, and P2W7 block ligand binding allosterically by stabilizing the angle of the bend in the bent conformation. Thus, a switchblade-like movement of the integrin leg is indispensable for the affinity regulation of αVβ3 integrin.

Introduction

Integrins are a family of α/β heterodimeric transmembrane cell surface receptors that mediate the cell-extracellular matrix and cell-cell interactions. The hallmark of integrin-dependent adhesive interactions is their regulation by intracellular signaling events (inside-out signaling). In addition to mediating adhesive interactions, liganded integrins initiate signals inside the cell to modify cell behavior (outside-in signaling) [1]. This integrin-mediated bidirectional signaling is closely associated with the structural rearrangement of the integrin itself. The crystal structure of the extracellular domains of αVβ3 and αIIbβ3 integrin revealed that the α chain consists of the N-terminal β-propeller domain followed by the thigh, calf-1, and calf-2 domains and that the β chain consists of the PSI, βA, hybrid, four EGF, and βT domains [2,3]. The β-propeller and the βA domains non-covalently associate with each other to form a globular head that is observable using conventional electron microscopy (EM) [4]. By contrast, the thigh, calf-1, and calf-2 domains of the α chain and the PSI, hybrid, EGF, and βT domains of the β chain form a leg-like region, respectively. The most striking feature revealed in the crystal structure is the orientation of the head. The two legs in the crystal structure fold back at a 135-degree angle between the thigh and the calf-1 domains and between the EGF-1 and EGF-2 domains, unlike the straight leg observed using conventional EM. Conse-

quently, the head region points downward, facing the plasma membrane. The discrepancies between these two structures were reconciled by a high-resolution EM image of the extracellular domains of recombinant αVβ3 integrin [5]. These observations revealed that αVβ3 could adopt multiple distinct structures, including the bent and the extended conformers observed in the crystal structure and conventional EM studies, respectively. Since Mn^{2+} and ligand peptide significantly increased their number, the extended form appeared to represent the high-affinity state, and the bent conformer was thought to represent the low-affinity state. Thus, the transition from one conformer to the other (the so-called switchblade-like movement) might account for the affinity regulation of the integrin. Consistent with these findings, genetically engineered αIIbβ3 constrained in the bent state interfered with the binding of macromolecular ligands, while αIIbβ3 constrained in the extended state exhibited maximal activation [6,7]. Finally, αIIbβ3 embedded in nanodiscs underwent extension in the presence of a talin head domain that binds to the β3 cytoplasmic domain, suggesting that the switchblade-like transition actually occurs during inside-out signaling [8]. Aside from the switchblade-like movement, substantial structural rearrangement has been observed in the head region. An EM study of α5β1 integrin complexed with a fibronectin fragment revealed that the β hybrid domain swings out upon ligand binding [9]. The

crystal structures of αIIbβ3 head regions complexed with short ligand peptides or ligand mimetics have provided detailed information [3,10]. This swing-out movement is accompanied by the rearrangement of the ligand-binding and/or cation-binding loops in the βA domain, thereby regulating ligand binding. In agreement with these findings, attempts to constrain the movement of the hybrid domain in a swing-out (open headpiece) or a swing-in (closed headpiece) position revealed that this movement is critical not only for β3 integrin activation [7,11], but also for β1 and β2 integrins [12–14]. Thus, these results suggest that extension and an open headpiece conformation are independently required for high-affinity ligand binding.

However, contradicting reports have suggested that integrin extension is not an essential event for ligand binding. The crystal structure of αVβ3 complexed with a small peptide ligand revealed that the bent conformer is capable of binding a ligand [15]. Understandably, αVβ3 was unable to undergo gross structural rearrangements upon ligand binding under the constraints of the crystal lattice in this experiment. However, a single particle analysis of αVβ3 complexed with a recombinant fibronectin fragment has shown that αVβ3 can bind to a macromolecular ligand when it is in a bent state in the presence of Mn^{2+} [16]. The measurement of fluorescent energy transfer between the mAb bound to the β-propeller domain and the plasma membrane in live cells revealed that αVβ3 remains in a bent conformation when activated by Mn^{2+} or an activating mutation [17]. These lines of evidence suggest that the bent conformer is capable of binding not only small ligands, but also macromolecular ligands without undergoing substantial structural rearrangements of αVβ3 integrin.

Most of the structural and/or functional studies on integrins described above have been performed using genetically manipulated molecules. Thus, it is impossible to negate the possibility that those manipulations could have an unexpected effect on the folding/gross structure of the molecule. If this were the case, interpretation of the whole data would be jeopardized. For these reasons, alternative approach is required to investigate the mechanism of integrin activation. In this study, we examined epitopes for numerous anti-αVβ3 monoclonal antibodies, some of which have been known to interfere with the αVβ3-based functions of cells. To our surprise, some of the function-blocking mAbs bound to the thigh domain of the αV chain, which does not contain a ligand-binding site. Further investigation using cells expressing human-to-mouse αV chimeras revealed that three mAbs shared an amino acid residue located above the α-genu as a common epitope. These mAbs inhibited fibrinogen binding to αVβ3-expressing cells to varying extents. To elucidate the blocking mechanism of these mAbs, αVβ3 constrained in the extended conformation was engineered. This mutant αVβ3 was highly active, compared with the wild-type, and bound fibrinogen even in the presence of Ca^{2+}, which is known to inhibit αVβ3-ligand interactions. All the genu-binding mAbs failed to inhibit fibrinogen binding to the mutant αVβ3, suggesting that these mAbs block ligand binding allosterically by restricting the angle of the bend. Our findings are consistent with the hypothesis that the ligand-binding activity of integrin can be regulated by the switchblade-like movement of the leg structure of integrin centering on the genu.

Materials and Methods

Antibodies and Reagents

Normal mouse IgG was purchased from Sigma-Aldrich (St. Louis, MO). The mAbs against αV (CD51), β3 (CD61), or αVβ3

complex (CD51/CD61) were obtained from the following sources. Non-functional anti-β3 mAb VNR5-2 has been previously characterized [18]. Anti-β3 mAb SZ21 and anti-αV mAbs AMF-7 [19] and 69-6-5 [20] were purchased from Beckman Coulter (Fullerton, CA). Anti-αV mAbs 17E6 [21] and P2W7 [22] were purchased from Calbiochem (La Jolla, CA) and R&D Systems (Minneapolis, MN), respectively. Anti-αV mAbs P3G8 [23], M9 [24], and anti-αVβ3 complex-specific mAbs LM609 [25] were purchased from Chemicon International (Temecula, CA). Anti-αVβ3 complex-specific mAb 23C6 [26] were purchased from BD Pharmingen (San Diego, CA). Hybridomas producing anti-β3 mAb 7E3 [27] and anti-αVβ3 complex mAb 10C4.1.3 [28] were obtained from the American Type Culture Collection (Manassas, VA). RPE-conjugated goat anti-mouse polyclonal antibody was purchased from Biosource (Camarillo, CA). The synthetic peptide Gly-Arg-Gly-Asp-Ser (GRGDS) was purchased from the Peptide Research Institute (Osaka, Japan). Fluorescein-isothiocyanate (FITC) was purchased from Sigma-Aldrich (St. Louis, MO). Human fibrinogen was purchased from Enzyme Research Laboratories (South Bend, IN).

Construction of Mutant αV cDNA Clones

The full-length cDNAs for the integrin αV, αIIb and β3 subunits, which were generous gifts from Dr. Joseph C. Loftus (Mayo Clinic Scottsdale, AZ), were cloned into the mammalian expression vector pBJ-1, which was kindly provided by Dr. Mark Davis (University of California, San Francisco). The cDNAs for the αV/αIIb domain-swapping chimeras VT, VC1, and VC2 were created using the overlap extension PCR method. The cDNAs for the B/V, V/B, T, C1, and C2 chimeras have been described elsewhere [29]. The domain boundaries for each chimera were set as shown in Fig. 1. The cDNAs for the human-to-mouse αV mutants I441V, T460ICP (T460I/S462P), T460I, S462P, V486T, N492H, E496DV (E496D/L497V), Y515HN (Y515H/S516N), S520V, N524T, I527VF (I527V/S528F), I527V, S528F, L532Q, I539V, Y565Q, T571A, and I586V and the cDNA for αV-to-αIIb mutants Q456P, D457A, N458V, T460S, G465Q, A467K, L468T, and K469P and the cDNA for αV mutant Q589NAT (Q589N/H591T) were created using site-directed mutagenesis and a Transformer Site-Directed Mutagenesis Kit (BD Biosciences, San Jose, CA).

Cell Culture and Transfection

Chinese hamster ovary (CHO)-K1 cells, obtained from the American Type Culture Collection (Manassas, VA), were cultured in Dulbecco's modified Eagle's medium (Invitrogen, Carlsbad, CA) supplemented with 10% fetal calf serum (Hyclone, Logan, UT), 1% penicillin and streptomycin (Invitrogen, Carlsbad, CA), and 1% non-essential amino acids (Sigma-Aldrich, St. Louis, MO) and maintained at 37°C in a humidified incubator supplemented with 5% CO_2. Fifty micrograms of αV or αIIb cDNA construct was co-transfected with 50 μg of β3 cDNA construct into CHO-K1 cells using electroporation. After 48 hours, the cells were detached and used in further experiments.

Flow Cytometry

Cells were detached with phosphate-buffered saline (PBS) containing 3.5 mM EDTA. After washing, the cells were incubated with 10 μg/mL of mAb in modified HEPES-Tyrode buffer (HTB; 5 mM HEPES, 5 mM glucose, 0.2 mg/mL bovine serum albumin, 1× Tyrode's solution) supplemented with 1 mM $CaCl_2$ and 1 mM $MgCl_2$ for 30 min at 4°C. After washing, the cells were incubated with an RPE-conjugated F(ab')₂ fragment of goat anti-mouse IgG for 30 min at 4°C. After washing, the cells
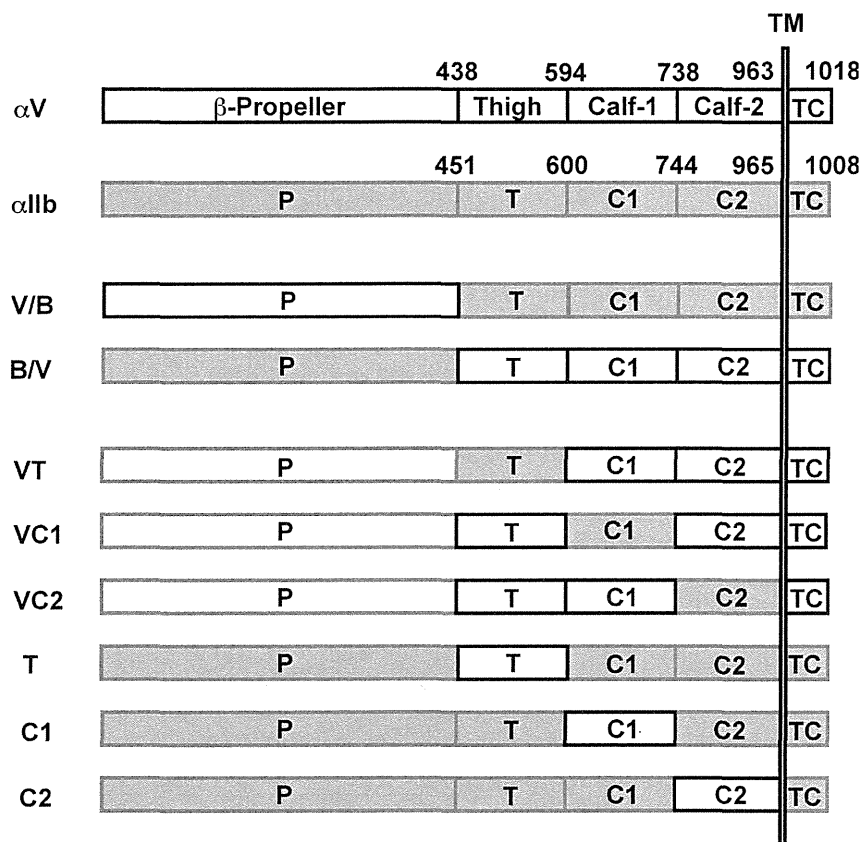
83

TM

αV — | 438 | 594 | 738 | 963 | 1018 |
β-Propeller | Thigh | Calf-1 | Calf-2 | TC

αIIb — | 451 | 600 | 744 | 965 | 1008 |
P | T | C1 | C2 | TC

V/B — P | T | C1 | C2 | TC

B/V — P | T | C1 | C2 | TC

VT — P | T | C1 | C2 | TC

VC1 — P | T | C1 | C2 | TC

VC2 — P | T | C1 | C2 | TC

T — P | T | C1 | C2 | TC

C1 — P | T | C1 | C2 | TC

C2 — P | T | C1 | C2 | TC

Figure 1. Schematic representation of αV/αIIb chimeras. The abbreviations P, T, C1, C2, and TC in the figure stand for β-propeller, thigh, calf-1, calf-2, and transmembrane-cytoplasmic domain, respectively. The numbers indicate the domain boundaries used to create the chimeras.
doi:10.1371/journal.pone.0066096.g001

were resuspended in HEPES-buffered saline (HBS; 10 mM HEPES, 150 mM NaCl, pH 7.4) containing 1 mM $CaCl_2$ and 1 mM $MgCl_2$; the fluorescence was then measured using a FACSCalibur (BD Biosciences, San Jose, CA).

Fibrinogen Binding Assay

FITC labeling of human fibrinogen was performed as previously described [30]. Forty-eight hours after transfection, the cells were detached and washed once with HTB. The αVβ3-transfected cells were incubated with anti-β3 mAb VNR5-2 followed by incubation with an RPE-conjugated $F(ab')_2$ fragment of goat anti-mouse IgG. After washing, the cells were incubated with 340 μg/mL of FITC-labeled fibrinogen with or without 1 mM GRGDS peptide in HTB containing 1 mM $CaCl_2$ and 1 mM $MgCl_2$ or containing 2 mM $MgCl_2$ and 5 μM EGTA for 2 hours at 4°C. After washing, fluorescence was measured using a FACSCalibur. The mean Fbg binding (FL1) to cell populations expressing a high β3 (FL2>1000) was calculated. Background binding in the presence of 1 mM GRGDS peptide was subtracted to obtain the specific binding. In the monoclonal antibody inhibition assays, after staining with primary and secondary antibodies, the cells were resuspended in HTB. Then an equivalent volume of 200 μg/mL mAb solution in PBS was added to yield a final concentration of 100 μg/mL. As a control, an equivalent volume of PBS was added instead of the mAb solution. Then FITC-labeled fibrinogen, $MgCl_2$, and EGTA were added at concentrations of 340 μg/mL, 2 mM, and 5 μM, respectively. The specific fibrinogen binding was normalized using the expression of αVβ3 on the cell

surface and by dividing the MFI (FL1) obtained in the presence of each mAb by the MFI (FL2) of the gated cell population.

Immunoprecipitation

Biotin labeling of the cell surface protein was performed using Sulfo-NHS-Biotin (Thermo Scientific, Rockford, IL), following the manufacturer's instructions. Cells were lysed in 1 mL of lysis buffer (100 mM n-octylglucopyranoside, 20 mM N-ethyl maleimide, 1 mM PMSF, 25 mM Tris-HCl, and 150 mM NaCl, pH 7.4). After removing the insoluble material by centrifugation, the supernatant was used for further analysis. Two hundred microliters of cell lysate was precleared by adding 1 μg of mouse IgG, together with 20 μL of Protein G agarose beads. After centrifugation, the supernatant was recovered and further incubated with 1 μg of VNR5-2, together with 20 μL of Protein G agarose beads overnight at 4°C. Then the supernatant was discarded, and the remaining Protein G agarose beads were washed 3× with washing buffer (25 mM Tris-HCl, 150 mM NaCl, 0.01%TritonX-100 [pH 8.0]). After washing, the samples were subjected to 7.5% SDS-PAGE, transferred to a polyvinylidene difluoride membrane, probed with horseradish peroxidase-conjugated avidin, and detected using chemiluminescence with the West Pico Chemiluminescent Substrate (Thermo Scientific, Rockford, IL).

84

Table 1. MAb binding to cells expressing tail-swapping chimeras.

	mIgG	10C4	23C6	LM609	17E6	69-6-5	AMF-7	M9	P2W7	P3G8	SZ21
CHO	5.26	4.77	4.34	4.48	4.94	5.23	3.57	3.15	18.99	4.25	3.63
β3	2.72	55.83	70.09	61.93	3.64	4.66	2.92	3.93	4.08	5.84	49.89
αVβ3	3.47	61.09	77.73	68.92	67.32	64.4	64.17	71.05	57.59	63.15	54.52
αIIβ3	3.92	57.69	58.25	65.47	3.66	4.25	3.07	4.08	4.61	5.56	51.73
V/B	4.18	58.73	69.11	61.9	53.13	45.19	3.08	3.78	6.00	6.36	52.16
B/V	4.24	51.6	63.63	57.3	7.11	6.44	58.39	63.47	49.97	55.63	49.16

MAb binding to cells expressing wild-type human β3 (β3), wild-type human αVβ3 (αVβ3), wild-type human αIIbβ3 (αIIbβ3), tail-swapping mutants (V/B, B/V), and to parent CHO cells (CHO) was examined. The numbers represent the percentage of the cell population stained with each mAb.
doi:10.1371/journal.pone.0066096.t001

Results

Epitope for functional anti-αV mAb is localized close to the α-genu

To probe the regulatory mechanism of integrin activation, epitopes for numerous anti-αVβ3 mAbs were examined. For this purpose, we generated a series of αV/αIIb chimeras. The B/V, V/B, T, C1, and C2 chimeras have been previously described [29]. Additionally, we created the VT, VC1, and VC2 chimeras in the present study (Fig. 1). These chimeric α chains were expressed together with the wild-type β3 chain in CHO cells, and the binding of a panel of mAbs to these cells was examined using FACS. All nine anti-αVβ3 mAbs that were tested bound to cells expressing wild-type αVβ3 but not to cells expressing αIIbβ3 or to parent CHO cells, with the exception of 10C4, 23C6, and LM609, which showed a partial reactivity with cells expressing αIIbβ3 (Table 1). However, the MFI values obtained for these 3 mAbs with αIIbβ3-expressing cells were significantly lower than the MFI values obtained with αVβ3-expressing cells (data not shown). In addition, these 3 mAbs also bound to cells expressing wild-type β3 alone. These results suggested that 10C4, 23C6, and LM609 cross-reacted with the hamster αV/human β3 hybrid. The other mAbs (AMF-7, M9, P2W7, and P3G8) bound to cells expressing B/V, but not to cells expressing V/B. In contrast, 17E6 and 69-6-5 bound to cells expressing V/B, but not to cells expressing B/V (Table 1). These results clearly indicated that the epitopes for mAbs 17E6 and 69-6-5 are contained in the N-terminal β-propeller domain and that the epitopes for mAbs AMF-7, M9, P2W7, and P3G8 are contained in the C-terminal leg region, consisting of the thigh, calf-1, and calf-2 domains. On the other hand, the mAbs 10C4, 23C6, and LM609 bound to cells expressing B/V as well as those expressing V/B. The MFI obtained with B/V was equivalent to the value obtained with cells expressing β3 alone and was significantly lower than that obtained with V/B (data not shown). These results suggested that the epitopes for 10C4, 23C6, and LM609 are localized in the β-propeller domain, but not the leg region.

Understandably, all the head-binding mAbs block ligand binding. However, some of the leg-binding mAbs also reportedly block cell adhesion, despite the fact that they bind to sites distant from the ligand-binding domain. To explore the mechanism by which these mAbs affect the αVβ3-ligand interaction, we decided to further localize the epitopes for these mAbs. To determine which domains these four leg-binding mAbs bind, individual domain sequences were exchanged between the αV and the αIIb chains. The resulting domain-swapping chimeras (T, C1, C2, VT, VC1, and VC2) were expressed together with wild-type β3 in CHO cells. The reactivity of these mAbs with αVβ3 was lost only

when the αV thigh domain sequences were replaced with the corresponding αIIb sequences (VT). In contrast, these mAbs gained reactivity with αIIbβ3 when the αIIb thigh domain sequences were replaced by the corresponding αV sequences (T) (Table 2). These results clearly indicated that the epitopes for the leg-binding mAbs are entirely confined in the thigh domain of the αV chain, and not in the calf-1 or calf-2 domains.

To further localize the epitopes for these leg-binding mAbs, short stretches of amino acid sequences in the thigh domain of human αV were replaced with the corresponding mouse αV sequences. The amino acid sequences of the mouse αV thigh domain differ from those of the human αV at 18 positions (Fig. 2). We initially created 14 human-to-mouse αV mutants and expressed them with wild-type β3 in CHO cells. As shown in Table 3, AMF-7, M9, and P2W7 failed to bind to cells expressing the T460ICP mutant, whereas P3G8 did not bind to cells expressing the I527VF mutant. None of the other mutations had a significant impact on the binding of these mAbs. The amino acid residues in the 460–462 and 527–528 regions were individually mutated to the corresponding mouse residues to identify the individual amino acid residues that were essential for the binding of these mAbs. As a result, S462P significantly blocked the binding of AMF-7, M9, and P2W7; S528F significantly blocked the binding of P3G8.

Sharing a common epitope does not necessarily imply that AMF-7, M9, and P2W7 bind to exactly the same site. The binding interfaces of AMF-7, M9, and P2W7 were further investigated using αV/αIIb chimeras. Although Ser-462 is located in a

Table 2. MAb binding to cells expressing domain-swapping chimeras.

	mIgG	AMF-7	M9	P2W7	P3G8	17E6	SZ21
CHO	7.83	5.86	5.72	15.51	5.78	5.91	4.8
αVβ3	5.6	68.11	78.41	63.75	67.97	76.32	59.23
VT	4.72	3.37	4.09	6.91	6.44	74.37	68.6
VC1	10.88	82.45	90.34	71.17	76.44	90.39	83.9
VC2	4.7	64.82	81.14	69.67	69.52	78.53	74.97
T	6.4	49.93	62.12	45.45	44.62	4.45	62.75
C1	5.87	3.8	4.03	5.82	6.37	4.05	61.79
C2	5.36	5.53	5.16	6.57	8.25	6.8	71.52

The numbers represent the percentage of the cell population stained with each mAb.
doi:10.1371/journal.pone.0066096.t002

85

```
human αV   441   ITVNAGLEVYPSILNQDNKTCSLPGTALKVSCFNVRFCLKADGKGVLPRKLNFQVELLLD   500
mouse αV   441   V................I.P.....................T.....H...DV...   500
human αIIb 454   VKASVQ.L.QD.-..PAV.S.V...Q.KTP.....IQM.VG.T.HNI-.Q..SLNA..Q..   511


human αV   501   KLKQKGAIRRALFLYSRSPSHSKNMTISRGGLMQCEELIAYLRDESEFRDKLTPITIFME   560
mouse αV   501   ..............HN...V...T..VF...Q......V...................   560
human αIIb 512   RQ.PRQG-..V.L.G.QQAGTTL.LDLGGKHSPI.HTTM.F....AD.....S..VLSLN   571


human αV   561   YRLDYRTAADTTGLQPILNQFTPANISRQAHIL   593
mouse αV   561   ....Q.....A..............V.......   593
human αIIb 571   VS.PPTE.----.MA.AVVLHGDTHVQE.TR.V   599
```

Figure 2. Comparison of amino acid sequences comprising the thigh domains. We show the amino acid residues 441 to 593 of the human and the murine αV chain compared with the homologous residues 454 to 599 of the human αIIb chain that differ from the human αV residues. The line connecting two Cys residues represents a disulfide link.
doi:10.1371/journal.pone.0066096.g002

disulfide-bonded loop, any involvement of other residues in the binding of these mAbs was impossible to determine using human-to-mouse chimeras. For this reason, amino acid residues 456–469 were mutated to the homologous residues in αIIb (Fig. 2) and expressed together with wild-type β3 in CHO cells. As shown in Fig. 3, these αV-to-αIIb mutations affected mAb binding differently. The binding of AMF-7, M9 and P2W7 were all impaired by G465Q and A467K. In addition, K469P significantly attenuated P2W7 binding. In the crystal structure, the disulfide-

Table 3. MAb binding to cells expressing human-to-mouse αV mutants.

	mIgG	AMF-7	M9	P2W7	P3G8	17E6	SZ21
CHO	3.62	2.56	2.95	13.3	3.2	4.07	1.16
WT	6.8	74.11	85.85	78.21	83.47	87.07	71.41
I441V	4.15	76.76	70.66	72.64	77.61	79.97	70.78
T460ICP	5.15	5.84	3.26	7.01	70.72	77.52	65.15
T460I	5.88	62.11	63.27	54.8	56.43	70.81	64.01
S462P	5.52	14.66	3.75	17.17	66.41	76.18	66.88
V486T	11.93	72.65	78.35	71.75	64.14	82.23	71.1
N492H	10.04	70.78	79	70.14	72.01	82.49	73.56
E496DV	14.9	73.25	76.95	67.31	75.08	75.01	58.72
Y515HN	8.47	59.79	67.31	59.04	65.69	66.81	50.75
S520V	8.33	65.13	72.76	61.29	73.55	71.38	60.68
N524T	12.98	60.75	69.31	58.6	65.03	66.37	57.98
I527VF	9.55	74.93	78.94	59.25	9.26	84.31	81.13
I527V	3.12	75.57	78.3	64.88	77.78	83.6	67.47
S528F	5.32	80.94	82.19	76.5	10.59	85.83	78.1
L532Q	26.68	62.2	77.22	58.2	62.38	76.84	71.26
I539V	13.13	73.98	67.01	57.12	68.84	76.24	64.92
Y565Q	11.64	70.1	77.22	64.52	71.32	80.13	72.63
T571A	27.84	68.76	69.91	54.89	59.55	75.22	75.28
I586V	9.99	70.96	78.21	61.16	70.96	68.54	76.34

The numbers represent the percentage of the cell population stained with each mAb. Bindings significantly lower than those for 17E6 or SZ21 are marked in red.
doi:10.1371/journal.pone.0066096.t003

bonded loop including Ser-462 is located above the α-genu (Fig. 4). Although Asp-457, Ala-467, and Lys-469 were separated in the primary structure, they were all located close to Ser-462 in the tertiary structure. On the other hand, Ser-528 was located on the side of the thigh domain distal to the α-genu (Fig. 4).

MAbs that bind to the α-genu affected ligand binding differently

To confirm the effect of these leg-binding mAbs on αVβ3-ligand interactions, fibrinogen binding to αVβ3-transfected cells was examined in their presence. FITC-labeled fibrinogen was incubated with αVβ3-expressing cells, and bound fibrinogen was measured using FACS. However, cells expressing the wild-type αVβ3 did not bind fibrinogen in the presence of 1 mM Mg^{2+} and 1 mM Ca^{2+}. Ca^{2+} is known to block αVβ3-ligand interactions, while Mg^{2+} supports such interactions. For this reason, 2 mM Mg^{2+} was utilized together with 5 μM EGTA to remove residual Ca^{2+} from the buffer. Under this cation condition, wild-type αVβ3 exhibited modest fibrinogen binding (Fig. 5A). Next, the effect of the anti-αVβ3 mAbs was examined using the same cation condition. The function-blocking anti-β3 mAb 7E3, which binds to the ligand-binding βA domain, significantly inhibited fibrinogen binding to cells expressing wild-type αVβ3. In contrast, anti-αV mAb P3G8 did not affect the binding. All three mAbs that bind above the α-genu blocked binding, albeit not as potently as 7E3 (Fig. 5B). A high-resolution EM study of recombinant αVβ3 revealed that the leg of the αV undergoes a bending/extending movement at the genu. These results suggest the possibility that the three mAbs might regulate the activity of αVβ3 by stabilizing the angle of the bend in favor of the bent conformation. To examine whether this situation actually occurs, fibrinogen binding was examined on cells expressing αVβ3 constrained in the extended conformation. To constrain αVβ3 in the extended state, an N-glycosylation site consisting of an N-X-T/S motif was introduced at amino acid residue Gln-589 of αV, which is located at the back of the genu (Fig. 4). The resulting Q589NAT mutation was thus expected to prevent αVβ3 from adopting a bent conformation. An SDS-PAGE analysis of the αVβ3 that immunoprecipitated with the anti-αV mAb revealed that the αV chain with the Q589NAT mutation migrated slightly more slowly than the wild-type αV, indicating the attachment of an extra glycan to the mutant (Fig. 6A). The homologous Q595NTT mutation in αIIb has been shown to constitutively activate αIIbβ3 [7].
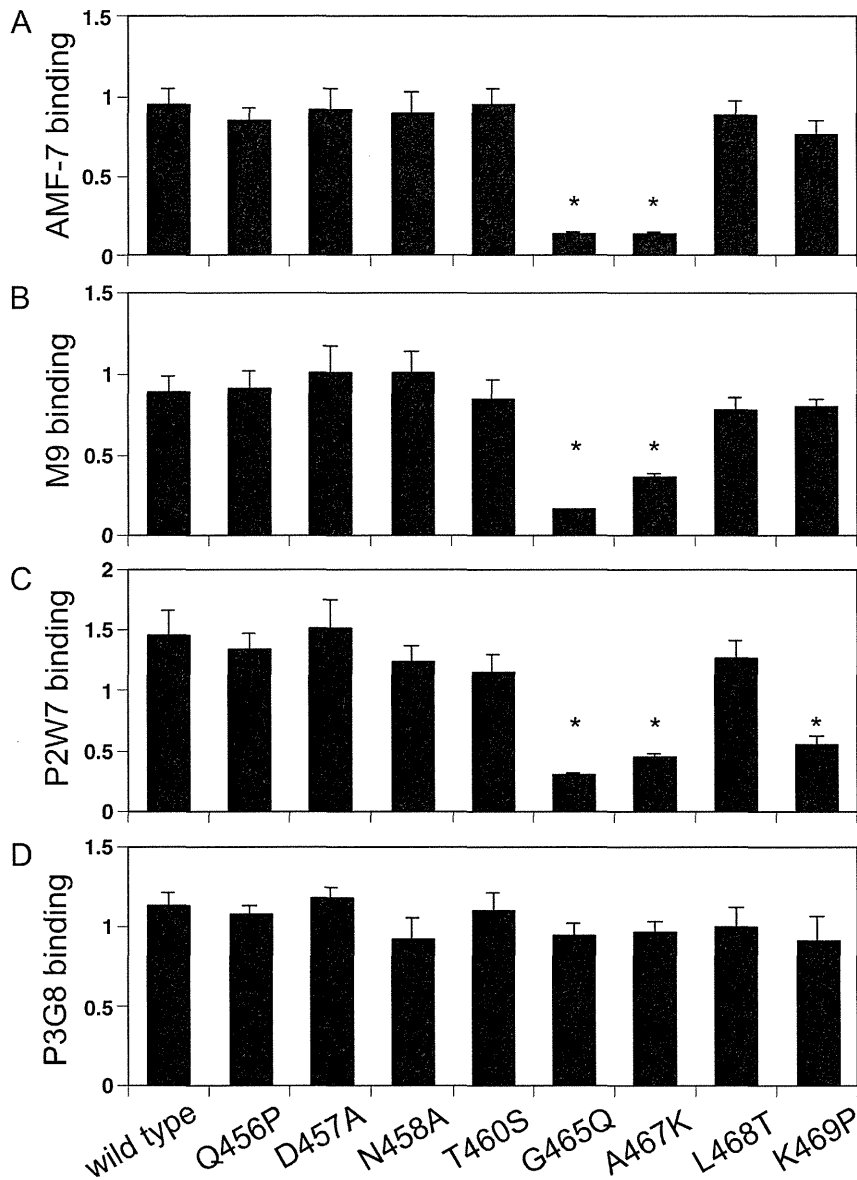
86

Figure 3. Effect of αV-to-αIIb mutation on the binding of the leg-binding mAbs. The amino acid residues 457–467 of the αV chain were individually mutated to the corresponding αIIb residues. The mutant αV was transiently expressed together with wild-type β3 in CHO cells, and the binding of mAbs to these cells was examined by FACS. The ratio of the MFI obtained from the whole cell population with each mAb to that obtained with 7E3 is shown as normalized binding. Asterisks indicate binding that was less than 50% of the wild type.
doi:10.1371/journal.pone.0066096.g003

Likewise, cells expressing the Q589NAT mutation exhibited robust fibrinogen binding, compared with cells expressing wild-type αVβ3 (Fig. 6B). Finally, the effect of anti-αVβ3 mAbs on fibrinogen binding to Q589NAT was examined using the same cation condition. As in the wild type, anti-β3 mAb 7E3 significantly blocked binding. In contrast, the mAbs AMF-7, M9, and P2W7 all failed to inhibit binding, as did P3G8 (Fig. 6C). It appeared possible that the Q589NAT mutation might directly affect the binding of these mAbs. To exclude this possibility, the reactivity of these mAbs was compared between cells expressing wild-type αVβ3 and cells expressing Q589NAT mutation. The result confirms that the Q589NAT mutation did not have any effect on the binding of AMF-7, M9, P2W7, or P3G8, as the binding of 7E3 (Fig. 7).

Discussion

We previously reported that extended αIIbβ3 had a high affinity for fibrinogen, whereas bent αIIbβ3 had a low affinity [7]. This previous study was based on a comparison of genetically engineered αIIbβ3, in which the three-dimensional structure was constrained either in the extended or bent conformation. However, these artificially engineered conformers do not necessarily represent native conformations that wild-type proteins adopt during physiological activation. For this reason, we used another approach to investigate the role of integrin extension in affinity regulation. In the present study, we showed that 1) the epitope for a group of anti-αV mAbs is located above the α-genu at which the leg of the integrin molecule bends, 2) these mAbs had a partial blocking effect on the αVβ3-ligand interaction, 3) constraining
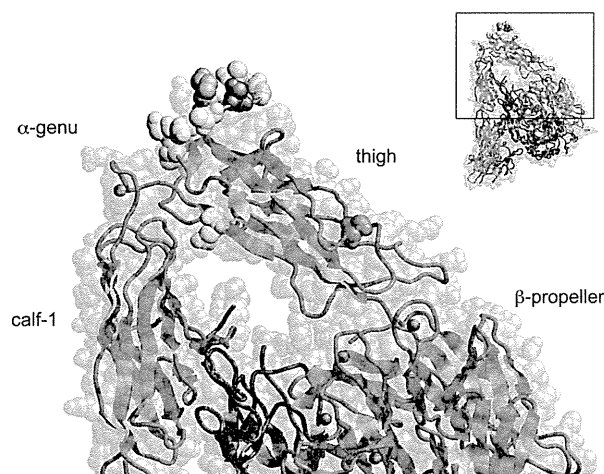
87

Figure 4. Locations of the critical residues for mAb binding in the three-dimensional αVβ3 structure. The crystal structure of the αV chain is shown by the blue spacefill representation, with its backbone shown by the ribbon. The β3 chain is shown by the gray ribbon. The epitope residues Ser-462 and Ser-528 are highlighted in red and magenta, respectively. Gly-465 and Ala-467 — which create a binding interface for AMF-7, M9, and P2W7 — are highlighted in yellow. Lys-469, important for P2W7 binding, is highlighted in orange. Residues that did not affect mAb binding when mutated are highlighted in white (see text). Gln-589 is highlighted in cyan. Note that Ser-462 is located above the α-genu, while Ser-528 is located on the side of the thigh domain distal to the α-genu.
doi:10.1371/journal.pone.0066096.g004

αVβ3 in its extended conformation resulted in robust activation, and 4) genu-binding inhibitory mAbs failed to block ligand binding to the extended αVβ3 molecule. Our results are consistent with the switchblade hypothesis (in which integrin extension increases the

affinity for ligands), rather than the dead-bolt theory (in which integrin activation is restrained by the βA/βT interaction, the disruption of which activates integrin without causing substantial extension).

Among the nine anti-αVβ3 mAbs that we tested, five of them — 10C4, 23C6, LM609, 17E6, and 69-6-5 — bound to the β-propeller domain, which composes a ligand-binding site with the βA domain. Consistently, these mAbs reportedly block the function of αVβ3 integrin [20,21,25,28]. On the other hand, among the four mAbs that bound to the thigh domain, AMF-7 reportedly inhibits cell adhesion [19] and M9 inhibits cell migration [24]. In contrast, P3G8 does not inhibit cell attachment to adhesive ligands [23], and no functional role has been reported for P2W7. We found these results surprising, since the thigh domain is located at a distance from the ligand-binding site. A fibrinogen binding study confirmed that AMF-7, M9, and P2W7 have a blocking effect on ligand binding, while P3G8 does not have any such effect (Fig. 5B). The effects of these mAbs were statistically significant. Notably, the function-blocking mAbs recognized the amino acid residue Ser-462, which is located within the disulfide-bonded loop above the α-genu, as a common epitope (Fig. 4). How can these genu-binding mAbs block ligand binding even though they bind at a site distant from the ligand-binding site? The genu-binding mAbs might block fibrinogen binding directly, depending on the orientation of the bound mAb. However, experiments using αV/αIIb domain-swapping chimeras suggest that the epitopes for the genu-binding mAbs are contained entirely within the thigh domain. These results indicate that the orientation of the bound mAbs relative to the bound ligand or the ligand-binding sites remains the same, regardless of the bent/extended states. If true, the genu-binding mAbs would likely block the extended αVβ3 as well. However, the results of our mAb blocking study on Q589NAT mutation suggest otherwise (Fig. 6C). These results seemed to indicate that the mAbs affected ligand binding via an allosteric mechanism, presumably by restricting the
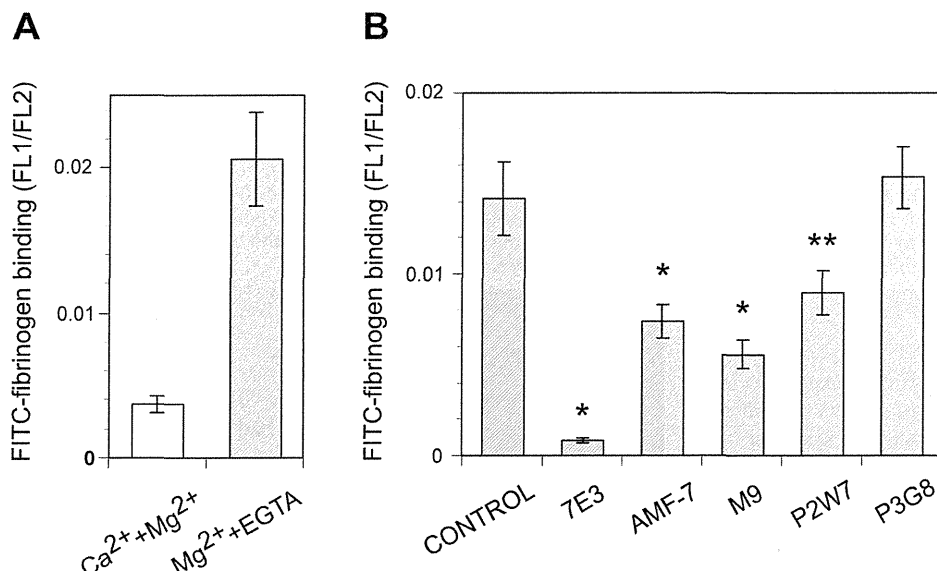

Figure 5. Effect of anti-αVβ3 mAbs on fibrinogen binding. A. FITC-fibrinogen binding to cells expressing αVβ3 in the presence of 1 mM Ca^{2+} and 1 mM Mg^{2+} (open column) or in the presence of 2 mM Mg^{2+} and 5 μM EGTA (hatched column) is shown. The ratio of the MFI (FL1) to the MFI (FL2) in the gated cell population was used to normalize the binding with the expression of αVβ3 on the cell surface. B. FITC-fibrinogen binding to cells expressing wild-type αVβ3 in the presence of 2 mM Mg^{2+} and 5 μM EGTA was examined. Binding in the presence of 100 μg/mL of the indicated mAb is shown in the hatched column. An equivalent volume of PBS, instead of the mAb solution, was included to obtain the control binding. The asterisks indicate statistically different binding abilities, compared with the control (*$P<0.01$, **$P<0.05$).
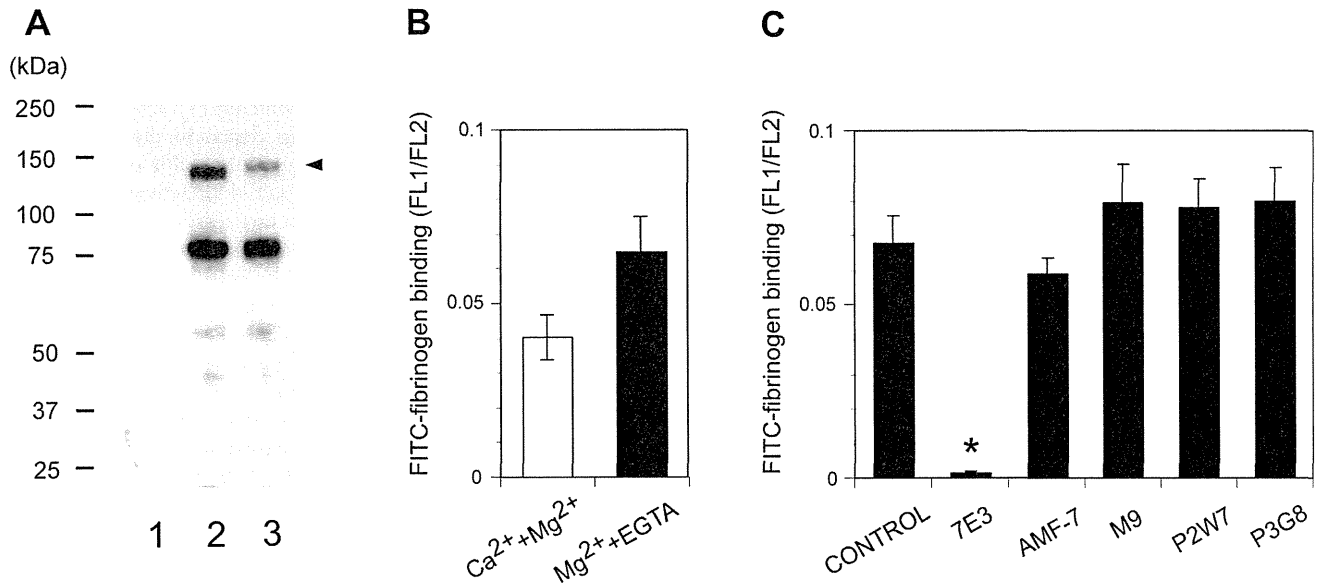doi:10.1371/journal.pone.0066096.g005

88

A

(kDa)

250 —

150 — ◄

100 —

75 —

50 —

37 —

25 —

1 2 3

B

FITC-fibrinogen binding (FL1/FL2)

0.1

0.05

0

$Ca^{2+}+Mg^{2+}$ $Mg^{2+}+EGTA$

C

FITC-fibrinogen binding (FL1/FL2)

0.1

0.05

0

CONTROL   7E3*   AMF-7   M9   P2W7   P3G8

Figure 6. Effect of integrin extension on the function of the anti-αVβ3 mAbs. A. SDS-PAGE analysis of αVβ3 expressed on CHO cells. Cell lysates from biotin-labeled cells expressing αVβ3 were immunoprecipitated with anti-αV mAb P2W7. The precipitates were subjected to a 7.5% non-reducing gel and visualized using chemiluminescence. The positions of the molecular weight markers are shown on the left side of panel. Lane 1, parent CHO; lane 2, wild-type αVβ3; lane 3, Q589NAT. Note that the αV carrying the Q589NAT mutation (arrowhead) migrated more slowly than the wild type. B. FITC-fibrinogen binding to cells expressing αVβ3 carrying the Q589NAT mutation was examined as described in Fig. 4A. Binding in the presence of 1 mM Ca^{2+} and 1 mM Mg^{2+} (open column) or in the presence of 2 mM Mg^{2+} and 5 μM EGTA (solid column) is shown. C. The effect of the anti-αVβ3 mAbs on fibrinogen binding to cells expressing αVβ3 carrying the Q589NAT mutation was examined, as described in Fig. 5B. Among the mAbs, only 7E3 significantly inhibited binding.
doi:10.1371/journal.pone.0066096.g006

angle of the bend. However, we lack conclusive evidence that Q589NAT mutation actually adopts an extended conformation at this point. Although our conclusion is based on a reasonable assumption, further investigation is required to confirm our claim. Consistent with this idea, the binding interfaces of these mAbs were located close to the possible thigh/calf-1 interface in the extended conformation (Fig. 4). This mechanism might partly explain why the blocking effects of these mAbs were relatively weak compared with that of 7E3, which binds to the βA domain and inhibits ligand binding competitively [31]. Interestingly, epitope residues for an activating mAb against the α chain of

αLβ2 integrin have been mapped to the back of the thigh domain, which is shielded in the bent conformation [32]. These previous results complement the present findings.

Numerous studies have shown that integrin extension is a prerequisite for integrin activation. A genetic approach in which integrin is constrained in a bent or extended conformation or in an open or closed headpiece conformation in αIIbβ3 and αLβ2 has indicated that both extension and an open headpiece are required for the binding of macromolecular ligands [6,7,13]. In agreement, another approach in which the αXβ2 conformation was constrained using functional mAbs has shown that an extended
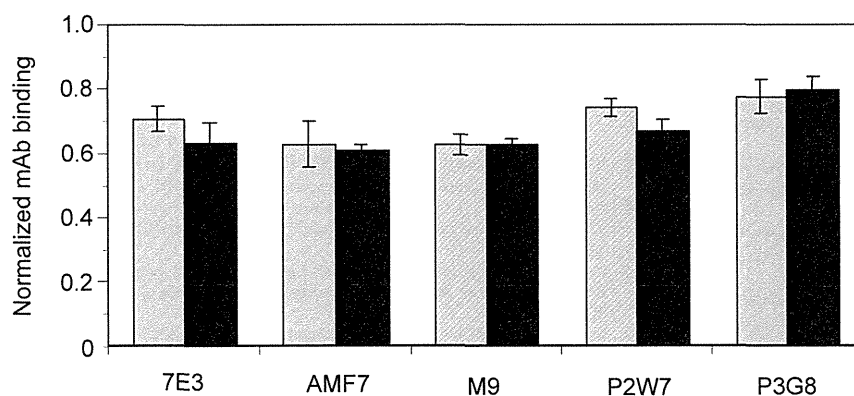
1.0

Normalized mAb binding

0.8

0.6

0.4

0.2

0

7E3   AMF7   M9   P2W7   P3G8

Figure 7. Effect of integrin extension on the binding of the anti-αVβ3 mAbs. Wild-type αV or αV carrying the Q589NAT mutation was transiently expressed together with wild-type β3 in CHO cells. The binding of function-blocking mAbs to these cells was examined by FACS. The MFI obtained from the whole cell population with each mAb was normalized by the MFI obtained with an anti-αV mAb 17E6 that represents the αV expression. There was no significant difference in the binding of leg-binding mAbs in cells expressing Q589NAT (solid column) as compared with cells expressing wild-type αV (hatched column).
doi:10.1371/journal.pone.0066096.g007

89

and open headpiece conformation represents a high-affinity state [14]. These studies clearly indicated that the extended conformation has a higher affinity for ligands than the bent conformation. Our results showed that αVβ3 was no exception. A substantial increase in fibrinogen binding was observed when αVβ3 was constrained in the extended conformation (Fig. 6B).

In contrast, several studies have suggested that the above is not true for αVβ3 integrin. Among them, the most compelling evidence showed that recombinant soluble αVβ3 could bind a fibronectin fragment while in a bent conformation [16]. This finding suggests that a bent and closed headpiece conformation represents a high-affinity state in αVβ3, which is completely opposite to the above-described results. The key to resolving this discrepancy may reside in the experimental conditions used in the experiments. As Blue et al. pointed out, whether integrin extension is required for ligand binding depends on the size of the ligand [6]. This situation probably arises because small ligands can gain access to a ligand-binding site in the proximity of the plasma membrane more easily than large ligands when the integrin is in its bent conformation. In other words, extension may regulate the accessibility of the ligand to integrin on the cell surface. If this is the case, extension might no longer be required in the absence of a plasma membrane. In agreement with this hypothesis, the recombinant αVβ3 lacked a transmembrane-cytoplasmic domain and the $FNIII_{7-10}$ fragment used in their experiment was relatively small and bound to αVβ3 at the C terminus, which would not interfere with the plasma membrane in the first place. However, considering the fact that $FNIII_{7-10}$ is located in the middle of the molecule, not at the terminus, the presence of the plasma membrane would hinder the binding of a native fibronectin molecule in the bent conformation. Thus, extension would be required for αVβ3 on the cell surface to interact with native fibronectin. Another important point is how the integrins are activated. In most experiments, Mn^{2+} is used to "activate" αVβ3 integrin. Although Mn^{2+} has been shown to induce extension in recombinant soluble αVβ3 [5], this might not be true for αVβ3 expressed on the cell surface with an intact interaction between the transmembrane-cytoplasmic domains of the α and the β subunits. Consistent with this idea, the height of αIIbβ3 reconstituted in liposomes did not change after Mn^{2+} activation [33]. In our experiments, the expression of an anti-LIBS epitope, which is preferentially expressed in liganded integrins, was not observed after Mn^{2+} activation, suggesting that extensive structural rearrangement did not occur because of Mn^{2+} alone (unpublished data). A comparison of the crystal structures of liganded and

unliganded αVβ3 has revealed that the rearrangement of the cation/ligand binding sites occurs without a swing-out in the presence of Mn^{2+} [2,15]. A similar rearrangement was accompanied by the swing-out of the hybrid domain in a liganded αIIbβ3 headpiece that lacked the lower leg region in the presence of Ca^{2+}/Mg^{2+} [3]. These results suggest that although an open headpiece conformation might be required for activation in Ca^{2+}/Mg^{2+}, such a conformation might not be necessary in Mn^{2+}. If this is the case, a bent and closed headpiece conformation could bind macromolecular ligands as long as the proximity of the plasma membrane did not prevent ligand access. Thus, integrins could bind ligands in the bent and closed headpiece conformation under specific experimental conditions. However, in physiological settings, extension and open headpiece conformation are both indispensable for high-affinity ligand interactions. It would be interesting to examine whether a closed headpiece conformer binds ligand in the presence of Mn^{2+}. In addition, the direct interaction of a soluble bent conformer with a ligand would have to be established to substantiate the hypothesis described above.

Our results and those of others indicate that the extended conformation has a higher affinity for ligands than the bent conformation, and nothing more. Although integrins fixed in a completely bent or extended conformation can be engineered and examined, the intermediate conformations between these two extremes are difficult to recreate experimentally. For this reason, no information is available regarding how much extension is needed to allow ligand binding. In other words, complete extension may not be necessary for initial ligand binding. This idea may explain why no substantial differences in the fluorescent donor-accepter separation distance between the fluorescent dye-labeled membrane and the fluorescent dye-labeled mAb bound to the β-propeller domain were detected between wild-type and a constitutively active mutant of αVβ3 [17]. Instead, an external force applied to the head region may be required to accomplish extension, as simulations of the molecular dynamics of αVβ3 have suggested [34]. Such forced extension may greatly stabilize integrin-ligand interactions [35]. Taken together, the present findings suggest that the switchblade-like movement of the integrin leg regulates the αVβ3-ligand interaction.

Author Contributions

Conceived and designed the experiments: TK. Performed the experiments: ST YS. Analyzed the data: TK SA. Contributed reagents/materials/analysis tools: MH YK YI. Wrote the paper: TK.

References

1. Hynes RO (2002) Integrins: bidirectional, allosteric signaling machines. Cell 110: 673–687.
2. Xiong JP, Stehle T, Diefenbach B, Zhang R, Dunker R, et al. (2001) Crystal structure of the extracellular segment of integrin alpha Vbeta3. Science 294: 339–345.
3. Xiao T, Takagi J, Coller BS, Wang JH, Springer TA (2004) Structural basis for allostery in integrins and binding to fibrinogen-mimetic therapeutics. Nature 432: 59–67.
4. Weisel JW, Nagaswami C, Vilaire G, Bennett JS (1992) Examination of the platelet membrane glycoprotein IIb-IIIa complex and its interaction with fibrinogen and other ligands by electron microscopy. J Biol Chem 267: 16637–16643.
5. Takagi J, Petre BM, Walz T, Springer TA (2002) Global conformational rearrangements in integrin extracellular domains in outside-in and inside-out signaling. Cell 110: 599–511.
6. Blue R, Li J, Steinberger J, Murcia M, Filizola M, et al. (2010) Effects of limiting extension at the alphaIIb genu on ligand binding to integrin alphaIIbbeta3. J Biol Chem 285: 17604–17613.
7. Kamata T, Handa M, Ito S, Sato Y, Ohtani T, et al. (2010) Structural requirements for activation in alphaIIb beta3 integrin. J Biol Chem 285: 38428–38437.
8. Ye F, Hu G, Taylor D, Ratnikov B, Bobkov AA, et al. (2010) Recreation of the terminal events in physiological integrin activation. J Cell Biol 188: 157–173.
9. Takagi J, Strokovich K, Springer TA, Walz T (2003) Structure of integrin alpha5beta1 in complex with fibronectin. Embo J 22: 4607–4615.
10. Springer TA, Zhu J, Xiao T (2008) Structural basis for distinctive recognition of fibrinogen gammaC peptide by the platelet integrin alphaIIbbeta3. J Cell Biol 182: 791–800.
11. Luo BH, Takagi J, Springer TA (2004) Locking the beta3 integrin I-like domain into high and low affinity conformations with disulfides. J Biol Chem 279: 10215–10221.
12. Luo BH, Strokovich K, Walz T, Springer TA, Takagi J (2004) Allosteric beta1 integrin antibodies that stabilize the low affinity state by preventing the swing-out of the hybrid domain. J Biol Chem 279: 27466–27471.
13. Tang XY, Li YF, Tan SM (2008) Intercellular adhesion molecule-3 binding of integrin alphaL beta2 requires both extension and opening of the integrin headpiece. J Immunol 180: 4793–4804.
14. Chen X, Xie C, Nishida N, Li Z, Walz T, et al. (2010) Requirement of open headpiece conformation for activation of leukocyte integrin alphaXbeta2. Proc Natl Acad Sci U S A 107: 14727–14732.
15. Xiong JP, Stehle T, Zhang R, Joachimiak A, Frech M, et al. (2002) Crystal structure of the extracellular segment of integrin alpha Vbeta3 in complex with an Arg-Gly-Asp ligand. Science 296: 151–155.

90

16. Adair BD, Xiong JP, Maddock C, Goodman SL, Arnaout MA, et al. (2005) Three-dimensional EM structure of the ectodomain of integrin {alpha}V{-beta}3 in a complex with fibronectin. J Cell Biol 168: 1109–1118.

17. Xiong JP, Mahalingham B, Alonso JL, Borrelli LA, Rui X, et al. (2009) Crystal structure of the complete integrin alphaVbeta3 ectodomain plus an alpha/beta transmembrane fragment. J Cell Biol 186: 589–600.

18. Tokuhira M, Handa M, Kamata T, Oda A, Katayama M, et al. (1996) A novel regulatory epitope defined by a murine monoclonal antibody to the platelet GPIIb-IIIa complex (alpha IIb beta 3 integrin). Thromb Haemost 76: 1038–1046.

19. de Vries JE, Keizer GD, te Velde AA, Voordouw A, Ruiter D, et al. (1986) Characterization of melanoma-associated surface antigens involved in the adhesion and motility of human melanoma cells. Int J Cancer 38: 465–473.

20. Lehmann M, Rabenandrasana C, Tamura R, Lissitzky JC, Quaranta V, et al. (1994) A monoclonal antibody inhibits adhesion to fibronectin and vitronectin of a colon carcinoma cell line and recognizes the integrins alpha v beta 3, alpha v beta 5, and alpha v beta 6. Cancer Res 54: 2102–2107.

21. Mitjans F, Sander D, Adan J, Sutter A, Martinez JM, et al. (1995) An anti-alpha v-integrin antibody that blocks integrin function inhibits the development of a human melanoma in nude mice. J Cell Sci 108 (Pt 8): 2825–2838.

22. von Schlippe M, Marshall JF, Perry P, Stone M, Zhu AJ, et al. (2000) Functional interaction between E-cadherin and alphav-containing integrins in carcinoma cells. J Cell Sci 113 (Pt 3): 425–437.

23. Wayner EA, Orlando RA, Cheresh DA (1991) Integrins alpha v beta 3 and alpha v beta 5 contribute to cell attachment to vitronectin but differentially distribute on the cell surface. J Cell Biol 113: 919–929.

24. Friedlander DR, Zagzag D, Shiff B, Cohen H, Allen JC, et al. (1996) Migration of brain tumor cells on extracellular matrix proteins in vitro correlates with tumor type and grade and involves alphaV and beta1 integrins. Cancer Res 56: 1939–1947.

25. Cheresh DA (1987) Human endothelial cells synthesize and express an Arg-Gly-Asp-directed adhesion receptor involved in attachment to fibrinogen and von Willebrand factor. Proc Natl Acad Sci U S A 84: 6471–6475.

26. Horton MA, Lewis D, McNulty K, Pringle JA, Chambers TJ (1985) Monoclonal antibodies to osteoclastomas (giant cell bone tumors): definition of osteoclast-specific cellular antigens. Cancer Res 45: 5663–5669.

27. Coller BS (1985) A new murine monoclonal antibody reports an activation-dependent change in the conformation and/or microenvironment of the platelet glycoprotein IIb/IIIa complex. J Clin Invest 76: 101–108.

28. Chuntharapai A, Bodary S, Horton M, Kim KJ (1993) Blocking monoclonal antibodies to alpha V beta 3 integrin: a unique epitope of alpha V beta 3 integrin is present on human osteoclasts. Exp Cell Res 205: 345–352.

29. Kamata T, Handa M, Sato Y, Ikeda Y, Aiso S (2005) Membrane-proximal {alpha}/{beta} stalk interactions differentially regulate integrin activation. J Biol Chem 280: 24775–24783.

30. Kamata T, Irie A, Tokuhira M, Takada Y (1996) Critical residues of integrin alphaIIb subunit for binding of alphaIIbbeta3 (glycoprotein IIb-IIIa) to fibrinogen and ligand-mimetic antibodies (PAC-1, OP-G2, and LJ-CP3). J Biol Chem 271: 18610–18615.

31. Puzon-McLaughlin W, Kamata T, Takada Y (2000) Multiple discontinuous ligand-mimetic antibody binding sites define a ligand binding pocket in integrin alpha(IIb)beta(3). J Biol Chem 275: 7795–7802.

32. Xie C, Shimaoka M, Xiao T, Schwab P, Klickstein LB, et al. (2004) The integrin alpha-subunit leg extends at a Ca2+-dependent epitope in the thigh/genu interface upon activation. Proc Natl Acad Sci U S A 101: 15422–15427.

33. Ye F, Liu J, Winkler H, Taylor KA (2008) Integrin alpha IIb beta 3 in a membrane environment remains the same height after Mn2+ activation when observed by cryoelectron tomography. J Mol Biol 378: 976–986.

34. Chen W, Lou J, Hsin J, Schulten K, Harvey SC, et al. (2011) Molecular dynamics simulations of forced unbending of integrin alpha(v)beta(3). PLoS Comput Biol 7: e1001086.

35. Litvinov RI, Mekler A, Shuman H, Bennett JS, Barsegov V, et al. (2012) Resolving two-dimensional kinetics of the integrin alphaIIbbeta3-fibrinogen interactions using Binding-Unbinding Correlation Spectroscopy. J Biol Chem.

91

Pharmacokinetic Study of Adenosine Diphosphate-Encapsulated Liposomes Coated with Fibrinogen γ-Chain Dodecapeptide as a Synthetic Platelet Substitute in an Anticancer Drug-Induced Thrombocytopenia Rat Model

KAZUAKI TAGUCHI,[1,5] HAYATO UJIHIRA,[1] HIROSHI WATANABE,[1,2] ATSUSHI FUJIYAMA,[3] MAMI DOI,[3] SHINJI TAKEOKA,[3] YASUO IKEDA,[3] MAKOTO HANDA,[4] MASAKI OTAGIRI,[1,5,6] TORU MARUYAMA[1,2]

[1]Department of Biopharmaceutics, Graduate School of Pharmaceutical Sciences, Kumamoto University, Chuo-ku, Kumamoto, 862–0973, Japan
[2]Center for Clinical Pharmaceutical Sciences, Kumamoto University, Chuo-ku, Kumamoto, 862–0973, Japan
[3]Department of Life Science and Medical Bioscience, Graduate School of Advanced Science and Engineering, Waseda University, Wakamatsu, Shinjuku-ku, Tokyo, 162–8480, Japan
[4]Department of Transfusion Medicine & Cell Therapy, Keio University, Shinjuku-ku, Tokyo, 160–8582, Japan
[5]Faculty of Pharmaceutical Sciences, Sojo University, Nishi-ku, Kumamoto, 862–0082, Japan
[6]DDS Research Institute, Sojo University, Nishi-ku, Kumamoto, 862–0082, Japan

ABSTRACT: A fibrinogen γ-chain (dodecapeptide HHLGGAKQAGDV, H12)-coated, adenosine diphosphate (ADP)-encapsulated liposome [H12-(ADP)-liposome] was designed to achieve optimal performance as a homeostatic agent and expected as a synthetic platelet alternative. For the purpose of efficient function as platelet substitute, H12-(ADP)-liposomes should potentially have both acceptable pharmacokinetic and biodegradable properties under conditions of an adaptation disease including thrombocytopenia induced by anticancer drugs. The aim of this study was to characterize the pharmacokinetics of H12-(ADP)-liposomes in busulphan-induced thrombocytopenic rats using ^{14}C, ^3H double radiolabeled H12-(ADP)-liposomes, in which the encapsulated ADP and liposomal membrane (cholesterol) were labeled with ^{14}C and ^3H, respectively. After the administration of H12-(ADP)-liposomes, they were determined to be mainly distributed to the liver and spleen and disappeared from organs within 7 days after injection. The encapsulated ADP was mainly eliminated in the urine, whereas the outer membrane (cholesterol) was mainly eliminated in feces. The successive dispositions of the H12-(ADP)-liposomes were similar in both normal and thrombocytopenic rats. However, the kinetics of H12-(ADP)-liposomes in thrombocytopenic rats was more rapid, compared with the corresponding values for normal rats. These findings, which well reflect the clinical features of patients with anticancer drug-induced thrombocytopenia, provide useful information for the development of the H12-(ADP)-liposomes for future clinical use. © 2013 Wiley Periodicals, Inc. and the American Pharmacists Association J Pharm Sci 102:3852–3859, 2013
Keywords: liposome; adenosine-diphosphate; dodecapeptide; disposition; thrombocytopenia; platelet substitute; biocompatibility; disease state; cancer chemthrapy

INTRODUCTION

Platelet transfusion represents one of the most essential prophylactic or therapeutic treatments for patients with thrombocytopenia caused by hematologic malignancies, or caused as a result of intensive chemotherapy and radiation used in the treatment of solid tumors. However, platelet transfusion can introduce a variety of complications such as virus infections, allergic reactions, and acute lung injuries. In addition, the shortage of donated platelets for blood transfusions has also become a serious issue because of the short shelf life of such products

(4 days in Japan and 5–7 days in the USA and Europe) and our aging society and the need for a stable supply in an emergency situation such as disasters and pandemics. To overcome these problems, attempts have been made to develop various platelet substitutes (artificial platelets), which consist of materials derived from blood components,[1] such as solubilized platelet membrane protein-conjugated liposomes (plateletsome),[2] infusible platelet membranes,[3] fibrinogen-coated albumin microcapsules (synthocyte),[4] red blood cells (RBC) with bound fibrinogen,[5] liposomes bearing fibrinogen,[6] arginine-glycine-aspartic acid peptide-bound RBC (Thromboerythrocyte)[7] and fibrinogen-conjugated albumin polymers.[8]

Adenosine diphosphate (ADP)-encapsulated liposomes modified with a dodecapeptide ([400]HHLGGAKQAGDV[411], H12) in the carboxy terminus of the fibrinogen γ-chain [H12-(ADP)-liposome] were developed as a new type of synthetic platelet alternative. The modification of H12-(ADP)-liposomes such as H12 and encapsulation with ADP enable them to specifically interact with activated platelets and stimulate platelet aggregation. It is well known that H12-(ADP)-liposomes bind to

glycoprotein IIb/IIIa on activated platelet membranes and accumulate between adherent platelets, analogous to fibrinogen in *in vitro* studies.[9–11] Furthermore, it was also reported that H12-(ADP)-liposomes specifically accumulate at the site of an injury *in vivo* and were reported to decrease bleeding time in a dose-dependent manner in both thrombocytopenic rat and rabbit models.[12–16] On the basis of these findings, it would be reasonable to conclude that H12-(ADP)-liposomes may be clinically acceptable for several disorders, such as injury, acute thrombocytopenic trauma with massive bleeding, and thrombocytopenia induced by drugs, as a platelet alterative.

Before new drugs are approved for clinical use, they are required to undergo a wide variety of evaluations, including physicochemical tests, preclinical studies, and clinical trials. Despite the accumulated basic evidence for the pharmacological effectiveness of H12-(ADP)-liposomes in the preclinical stage,[12–16] the pharmacokinetics of H12-(ADP)-liposomes have not been well characterized. Pharmacokinetic studies of H12-(ADP)-liposomes that have been reported to date have evaluated only their dispositions in normal animals including mice, rats, and rabbits.[17] In previous studies, it was reported that clinical conditions can affect the pharmacokinetics of liposomes.[18–20] Furthermore, Frank and Hargreaves reported that safe/toxicology and pharmacokinetic data, which are used to estimate pharmacokinetic studies in preclinical stages, accounts for approximately 40% of the failed attempts to develop new drug projects during clinical development.[21] Therefore, clarifying the pharmacokinetics of H12-(ADP)-liposomes in animal models of an adaptation disease (thrombocytopenia) should provide useful information, such as dosing regimens required for future clinical applications. In addition, the characteristics of the H12-(ADP)-liposomes developed in this study suggest that not only better pharmacological effects could be obtained, but the product may well have acceptable biodegradable properties (no accumulation or retention). These effects, however, need to be documented even under conditions of an adaptation disease (thrombocytopenia).

In the present study, we report on an evaluation of the pharmacokinetic properties of H12-(ADP)-liposomes and components derived from them in thrombocytopenia model rats produced as the result of anticancer drug therapy, which is a candidate for a disease that could be treated with H12-(ADP)-liposomes. For this purpose, we first created thrombocytopenia model rats induced by treatment with busulphan, anticancer drug used in the treatment of hematologic malignancies. We then evaluated the pharmacokinetic properties of the H12-(ADP)-liposomes and components in the thrombocytopenia model rats using ^{14}C, ^{3}H double radiolabeled H12-(ADP)-liposomes, in which the encapsulated ADP and membrane component (cholesterol) were labeled with ^{14}C and ^{3}H, respectively, and subsequently compared with the findings for those obtained using normal rats.

MATERIALS AND METHODS

Reagents

Cholesterol and 1,2-dipalmitoyl-*sn*-glycero-3-phosphatidylcholine were purchased from Nippon Fine Chemical (Osaka, Japan), and 2-distearoyl-*sn*-glycero-3-phosphatidylethanolamine-N-[monomethoxypoly(ethyleneglycol)] (5.1 kDa) was purchased from NOF (Tokyo, Japan). 1,5-

Dihexadecyl-*N*-succinyl-L-glutamate and H12–polyethyleneglycol (PEG)–Glu2C18, in which the fibrinogen γ-chain dodecapeptide (C-HHLGGAKQAGDV, Cys–H12) was conjugated to the end of the PEG–lipids, were synthesized as reported previously.[15] Busulphan was obtained from Sigma–Aldrich (St Louis, Missouri).

Animals

All animal experiments were undertaken in accordance with the guidelines, principles, and procedures of Kumamoto University for the care and use of laboratory animals. Experiments were carried out with male Sprague–Dawley rats (Kyudou Company, Kumamoto, Japan). All animals were maintained under conventional housing conditions, with food and water *ad libitum* in a temperature-controlled room with a 12-h dark/light cycle.

Preparation of Thrombocytopenic Rats

Thrombocytopenic rats induced by busulphan were created as previously reported by Yang et al.[22] with minor modifications. Typically, a busulphan solution was prepared at a final concentration of 10 mg/mL in PEG (average molecular weight 400). Rats were anaesthetized with ether and intraperitoneally injected on days 0 and 3 with equal amounts of a total dose of busulphan of 20 mg/kg.

Blood Sampling, Measurement of Hematology, and Serum Chemistry

At stipulated dates (0–14th day, 16th day, 18th day, and 20th day) after busulphan administration, blood samples (approximately 100 μL) for cell counts were obtained from the tail veins of ether-anaesthetized rats. Hematology analyses of venous samples were performed using KX-21NV (Sysmex, Kobe, Japan). The remaining venous blood samples obtained at days 0 and 10 after busulphan administration were centrifuged (1710g, 10 min) to obtain serum, which was used for the evaluation of serum chemistry [aspartate aminotransferase (AST), alanine aminotransferase (ALT), blood urea nitrogen (BUN), and creatinine]. AST and ALT activities levels were determined by using a transaminase C-II test kit from Wako Chemicals (Saitama, Japan). BUN and creatinine were determined by using a urea nitrogen-B test kit and LabAssay creatinine test kit from Wako Chemicals, respectively.

Preparation of ^{14}C, ^{3}H Double-Labeled H12-(ADP)-Liposomes

^{14}C-labeled H12-(ADP)-liposomes were first prepared under sterile conditions, as previously reported.[16] The diameter and Zeta potential of the ^{14}C-labeled H12-(ADP)-liposomes used in this study are regulated at 250 ± 50 nm and − 10 ± 0.9 mV, respectively. The ^{3}H labeling of ^{14}C-labeled H12-(ADP)-liposomes was carried out according to a previous report.[17] Before being used in pharmacokinetic experiments, all of the samples were mixed with unlabeled H12-(ADP)-liposomes.

Pharmacokinetic Studies in Thrombocytopenic Rats

Ten days after the administration of busulphan, 16 thrombocytopenic rats were anesthetized with ether and given a single injection of ^{14}C, ^{3}H-labeled H12-(ADP)-liposomes (10 mg lipids/kg). In all rat groups, four rats were selected to undergo a plasma concentration test. Under ether anesthesia,

approximately 200 μL blood sample from all administered groups were collected from the tail vein at multiple time points after the injection of the ^{14}C, ^{3}H-labeled H12-(ADP)-liposomes (3, 10, and 30 min; 1, 2, 3, 6, 12, and 24 h), and the plasma was separated by centrifugation (3000g, 5 min). After collecting the last blood sample (24 h), the rats were sacrificed and selected organs (kidney, liver, spleen, lung, and heart) were excised. Urine and feces were collected at fixed intervals in a metabolic cage. In addition, the four thrombocytopenic rats were randomly sacrificed and organs (kidney, liver, spleen, lung, and heart) were collected at 2 and 6 h and 7 days after an injection of ^{14}C, ^{3}H-labeled H12-(ADP)-liposomes at a dose of 10 mg lipids/kg.

Measurement of ^{14}C and ^{3}H Radioactivity

Plasma samples were solubilized in a mixture of Soluene-350 (Perkin Elmer, Yokohama, Japan) and isopropyl alcohol (at a ratio of 1/1) for 24 h at 50°C. The organ samples were rinsed with saline, minced, and solubilized in Soluene-350 for 24 h at 50°C. Urine and feces were also weighed and solubilized in Soluene-350. All samples were decolorized by treatment with a hydrogen peroxide solution after the Soluene-350 or isopropyl alcohol treatments. The ^{14}C, ^{3}H radioactivity was determined by liquid scintillation counting (LSC-5121; Aloka, Tokyo, Japan) with Hionic Fluor (Perkin Elmer).

Data Analysis

A noncompartment model was used for the pharmacokinetic analysis. Each parameter, half-life ($t_{1/2}$, h), mean residence time (h), area under the concentration–time curve (AUC, h % of dose/mL), clearance (CL, mL/h), distribution volume (mL), was calculated using the moment analysis program available on Microsoft Excel.[23] Data are shown as the mean ± SD for the indicated number of animals.

RESULTS AND DISCUSSION

The Creation of Thrombocytopenic Rats Induced by Busulphan

All rats survived the busulphan treatment and none were on the verge of death. Although the body weight of nontreatment rats were increased from 236.7 ± 5.8 to 310.6 ± 13.3 g, the weights of the busulphan-administered rats (thrombocytopenic rats) were only increased slightly, from 235.0 ± 4.2 to 289.5 ± 9.3 g at 10 days after busulphan administration.

Platelet counts of the rats that had been treated with busulphan were 91.0 ± 5.8 × 10^4 per microliter before busulphan administration, and declined significantly to 27.7 ± 2.7 × 10^4 per microliter at 10 days after busulphan administration, which meets the clinical criterion for thrombocytopenia (Fig. 1c). This severe thrombocytopenia was consistent with results reported in previous studies for busulphan treated rats at 10 days after busulphan administration.[14,16] Furthermore, the number of white blood cells and RBC slowly begun to decrease from 1 day after busulphan administration (Figs. 1a and 1b). In association with the decrease in RBC, the hemoglobin and hematocrit values were also altered (Table 1). However, the RBC-related parameters, including the mean corpuscular volume, mean corpuscular hemoglobin, and mean corpuscular hemoglobin concentration were not changed between before busulphan administration and 10 day after busulphan administration (Table 1). These results indicate that thrombocytopenia model rats are associated with the adverse effect (pancytopenia) of busulphan.
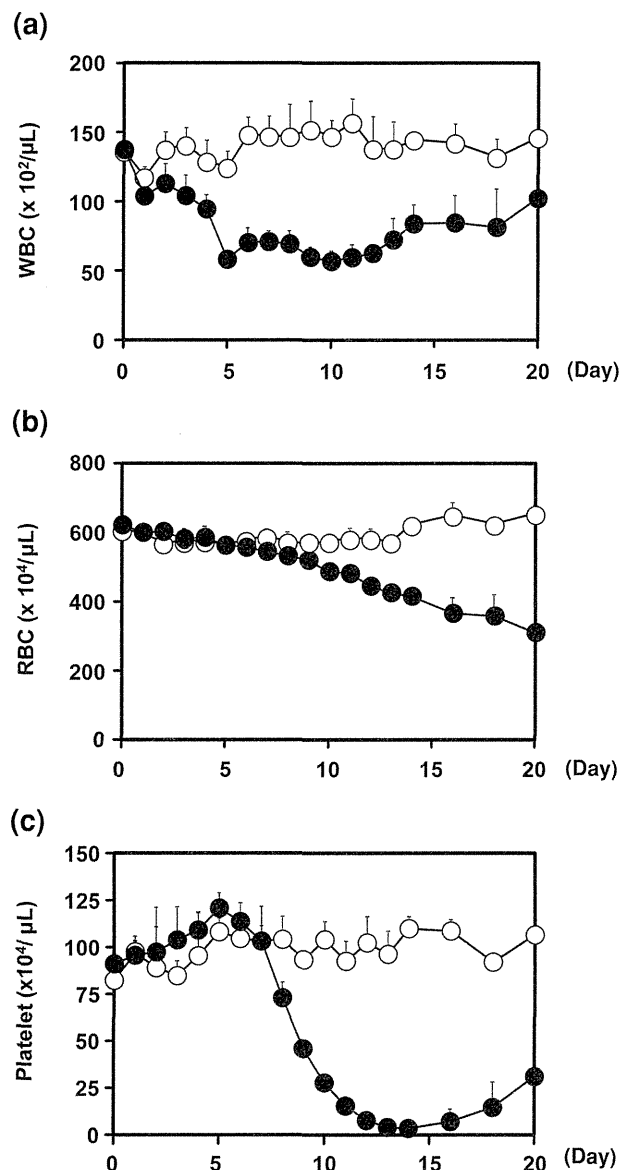

Figure 1. Time course for number of white blood cell (a), red blood cell (b), and platelet (c) in normal rats (open circle) and rats treated by busulphan at a total dose of 20 mg/kg (closed circle). Busulphan was interperitoneally injected to rats on days 0 and 3 with equal amounts of a total dose of busulphan of 20 mg/kg. Each point represents the mean ± SD (n = 4).

In clinical situations, patients with cancer, such as hematologic malignancies, receiving anticancer drugs frequently, need therapeutic platelet transfusions to counteract the effects of the anticancer drugs. Busulphan, one of the anticancer drugs used in the treatment of hematologic malignancies, induces thrombocytopenia as an adverse effect. Furthermore, the putative strategy for using H12-(ADP)-liposomes in a clinical situation is to alleviate the thrombocytopenia induced by anticancer drugs. Taken together, the rat model of thrombocytopenia created in the present study acceptably reflects this clinical situation. Therefore, a pharmacokinetic study of H12-(ADP)-liposomes was performed using busulphan-induced thrombocytopenia model rats at 10 days after busulphan administration.

Table 1. Changes in Hemoglobin, Hematocrit, and Other Red Blood Cells-Related Parameters in Normal Rats and Thrombocytopenic Rats at 0 and 10 Days After Busulphan Administration

	Nontreatment Rats		Thrombocytopenia Rats	
	Day (0)	Day (10)	Day (0)	Day (10)
Hemoglobin (g/dL)	13.1 ± 0.3	13.3 ± 1.4	13.5 ± 0.3	11.1 ± 0.2
Hematocrit (%)	39.2 ± 0.4	37.9 ± 0.3	40.5 ± 0.9	32.6 ± 0.7
MCV (fL)	71.0 ± 1.7	72.5 ± 1.0	71.6 ± 1.0	73.7 ± 0.8
MCH (pg)	23.7 ± 0.9	24.2 ± 0.2	24.0 ± 0.4	25.1 ± 0.4
MCHC (g/dL)	36.7 ± 1.2	36.7 ± 0.4	36.8 ± 0.3	37.3 ± 0.7

Blood samples (~100 µL) for cell counts were obtained from ether-anaesthetized rats treated with or without busulphan from a tail vein. Red blood cells-related parameters of venous samples were analyzed using automated blood cell counter.
Each value represents the mean ± SD ($n = 4$).
MCV, mean corpuscular volume; MCH, mean corpuscular hemoglobin; MCHC, mean corpuscular hemoglobin concentration.

Table 2. Serum Biochemical Parameters Representing Hepatic and Renal Function in Normal Rats and Thrombocytopenic Rats at 0 and 10 Days After Busulphan Administration

	Nontreatment Rats		Thrombocytopenia Rats	
	Day (0)	Day (10)	Day (0)	Day (10)
AST (IU/L)	32.0 ± 3.2	41.0 ± 5.6	31.0 ± 1.8	27.8 ± 3.3
ALT (IU/L)	8.2 ± 2.2	12.2 ± 1.1	7.7 ± 2.2	12.5 ± 1.6
CRE (mg/dL)	0.91 ± 0.05	1.08 ± 0.22	0.93 ± 0.17	0.90 ± 0.13
BUN (mg/dL)	15.7 ± 0.5	15.1 ± 0.8	17.2 ± 3.1	16.6 ± 3.1

Each value represents the mean ± SD ($n = 4$).
AST, aspartate aminotransferase; ALT, alanine aminotransferase; CRE, creatinine; BUN, blood urea nitrogen.

Figure 2. Plasma concentration curve of (a) ^{14}C and (b) 3H radiolabeled H12-(ADP)-liposome after intravenous injection at a dose of 10 mg lipids/kg to normal rats (open circle) and thrombocytopenic rats (closed circle). The data for the normal rats were cited from our previously reported paper.[17] Each point represents the mean ± SD ($n = 4$).

Serum Chemistry

It is well known that hepatic and renal function can have an effect on the pharmacokinetics of hepatic and renal clearing drugs, including liposomes. For example, the pharmacokinetics of hemoglobin vesicles (HbV), the liposomal characteristics of which are similar in terms of the liposomal structure to H12-(ADP)-liposomes, were reported to be altered in a rat model of chronic liver cirrhosis.[24] Our previous report demonstrated that the ADP encapsulated in H12-(ADP)-liposomes was mainly eliminated in the urine after being metabolized to allantoin, whereas the lipid components (cholesterol) were mainly eliminated in feces via bile.[17] Therefore, it is important to consider the effect of busulphan administration on hepatic and renal function before collecting pharmacokinetic data for thrombocytopenic rats induced by busulphan treatment.

In the present study, no changes in the parameters reflecting liver function (AST and ALT) were found at 10 days after busulphan administration (Table 2). In addition, BUN and creatinine levels, which reflect renal function, were also unchanged at 10 days after busulphan administration (Table 2). These results indicate that busulphan administration had no effect on the pharmacokinetics of H12-(ADP)-liposome with respect to changes in hepatic and renal function in busulphan-induced thrombocytopenia model rats.
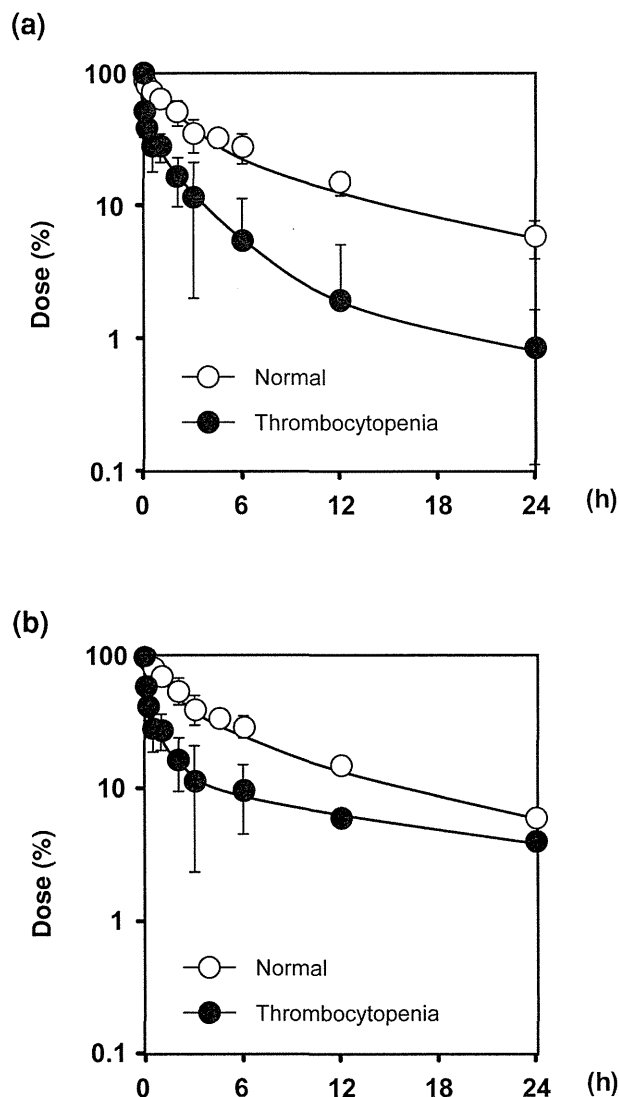
Pharmacokinetics of H12-(ADP)-Liposome Components in Normal and Thrombocytopenic Rats

Plasma Concentration

Figure 2 shows the time course for the plasma concentration of the ^{14}C, ^{3}H-labeled H12-(ADP)-liposomes that were injected into normal rats and thrombocytopenic rats at a dose of 10 mg lipid/kg, which was lowest recommended dosage to exert enough hematostatic effect in thrombocytopenic rats,[14,16] and Table 3 lists the pharmacokinetic parameters calculated from the data shown in Figure 2. The plasma concentration curves and pharmacokinetic parameters for ^{14}C radioactivity and ^{3}H radioactivity were different between normal rats and thrombocytopenic rats (Fig. 2 and Table 3). Accompanied by the change of plasma concentration curve, the $t_{1/2}$ for both ^{14}C radioactivity and ^{3}H radioactivity in thrombocytopenic rats